CrossMark

Northern Hemisphere extratropical winter cyclones variability over the 20th century derived from ERA-20C reanalysis

Filipa Varino[1] · Philippe Arbogast[2] · Bruno Joly[2] · Gwendal Riviere[3] · Marie-Laure Fandeur[4] · Henry Bovy[4] · Jean-Baptiste Granier[4]

Abstract

The multi-decadal variations of wintertime extra-tropical cyclones during the last century are studied using a vorticity-based tracking algorithm applied to the long-term ERA-20C reanalysis from ECMWF. The variability of moderate-to-deep extra-tropical winter cyclones in ERA-20C show three distinct periods. Two at the beginning and at the end of the century (1900–1935 and 1980–2010) present weak or no significant trends in the Northern Hemisphere as a whole and only some regional trends. The period in between (1935–1980) is marked by a significant increase in Northern Hemisphere moderate-to-deep cyclones frequency. During the latter period, polar regions underwent a significant cooling over the whole troposphere that increased and shifted poleward the mid-latitude meridional temperature gradient and the baroclinicity. This is linked to positive-to-negative shifts of the PDO between 1935 and 1957 and of the AMO between 1957 and 1980 which mainly reinforced the storm-track eddy generation in the North Pacific and North Atlantic regions respectively, as seen from baroclinic conversion from mean to eddy potential energy. As a result, both the North Pacific and North Atlantic extra-tropical storms increase in frequency during the two subperiods (1935–1957 and 1957–1980), together with other storm-track quantities such as the high-frequency eddy kinetic energy. In contrast, the first and third periods are characterized by a warming of the polar temperatures. However, as the stronger warming is confined to the lower troposphere, the baroclinicity do not uniformly increase in the whole troposphere. This may explain why the recent rapid increase in polar temperatures has not affected the behaviour of extratropical cyclones very much. Finally, the large magnitude of the positive trend found in moderate-to-deep cyclone frequency during the second period is still questioned as the period is marked by an important increase in the number of assimilated observations. However, the dynamical link between changes in cyclone frequency, changes in large-scale baroclinicity and ocean decadal variability found in the present study makes us confident on the sign of the detected cyclone trend.

1 Introduction

Mid-latitude cyclones are responsible for the distribution of moisture, temperature and precipitation in the middle latitudes and can produce severe economical and social damages. In the Northern Hemisphere (NH), two particular regions of storms crossing the North Atlantic (ATL) and Pacific (PAC) oceanic basins exist. These regions are known as the storm-track regions (Hoskins and Hodges 2002) and are well depicted by band-pass filters variance of 300 hPa meridional wind-fields (Blackmon et al. 1977; Chang et al. 2002). However, to get an information on the initiation, mature and decay stages of cyclones, cyclone tracking algorithms are more appropriate. These algorithms generally

✉ Filipa Varino
filipa.varino@meteo.fr

1 CNRM, UMR 3589, Météo-France/CNRS, Toulouse, France

2 CNRM, UMR 3589, Météo-France, Toulouse, France

3 LMD/IPSL, Département de Géosciences, ENS, PSL Research University, Ecole Polytechnique, Université Paris Saclay, Sorbonne Universités, UPMC Univ Paris 06, CNRS, Paris, France

4 SCOR, Paris, France

detect minima in mean sea level pressure (MSLP) or maxima in low-level vorticity and identify them as cyclones' centers. Then, the trajectory of each cyclone is computed by searching the nearest extrema in MSLP or vorticity at successive time steps. However, these methods have some limits. While MSLP can be affected by large scale systems, vorticity is more noisy and more sensitive to data resolution than MSLP. One advantage of the vorticity over MSLP is that it can detect extra tropical storms in its early states (Sinclair 1997; Hoskins and Hodges 2002). Some studies have shown that the choice of the variable together with those of the data resolution and type can change results on cyclones statistics significantly (Neu et al. 2013), especially their intensity (Ulbrich et al. 2009; Bader et al. 2011).

Several authors have compared results from different reanalysis and different tracking methods (Raible et al. 2008; Ulbrich et al. 2009; Tilinina et al. 2013; Neu et al. 2013; Wang et al. 2013, 2016; Chang and Yau 2015). In general, results obtained from reanalysis data are correlated but small changes can be observed due to the use of different methods and/or data resolution. Furthermore several shifts in results were found associated with an increase in assimilated observation and satellite data (Bengtsson 2004; Bromwich et al. 2007; Chang 2007; Wang et al. 2016).

Results in tracked cyclone statistics using reanalysis data in the NH largely differ from one study to another. Gulev et al. (2001) applied a tracking algorithm to NCEP/NCAR MSLP datasets for the JFM months between 1958 and 1999. They found a negative trend in the total number of cyclones in the ATL and PAC and an increase in strong cyclones on the western side of the storm tracks. Using the same NCEP/NCAR reanalysis, Chang and Fu (2002) performed a principal component analysis on the high-pass-filtered 300-hPa meridional wind variance and obtained a decrease in DJF cyclones until the 70s followed by an increase afterwards. Still using the same data and for the same winter months Paciorek et al. (2002) analysed the second half of the 20th century using a tracking algorithm cyclone on MSLP and different indexes as cyclone predictors. They found that there is an increase in intensity of cyclones but that the number of cyclones has not increased. The same increase in intensity was shown in the PAC by Graham and Diaz (2001) for NCEP/NCAR Dec–Mar months and by Wang et al. (2006) in NCEP/NCAR and ERA-40 reanalysis on the NH for the DJF months. This last one also found a shift on the storm tracks, and an increase in deep cyclones over western Europe (from tracked MSLP minimums). Similarly, McCabe et al. (2001) observed a decrease (increase) in mid-(high) latitude cyclone frequency on Nov–Mar months for the same reanalysed MSLP tracked data that goes in agreement with a possible poleward shift of the storm tracks. Trigo (2006) compared Dec–Mar results from ERA-40 and NCEP/NCAR and found an increase in intense cyclones in the ATL and

a northward shift of the ATL storm track. In conclusion, despite important discrepancies, most studies seem to agree with an increase in deep cyclones and in a poleward shift of the storm tracks during the second half of the 20th century.

While most studies focused on the recent decades, very few studies exist using long-term reanalysis data covering the whole 20th century, like 20CR from NOAA based on the ensemble Kalman filter approach with fifty six members and ERA-20C from the ECMWF based on the 4DVar approach where the background error covariances are sampled using an ensemble of 4DVar (Compo et al. 2011; Poli et al. 2016). Compared to NCEP/NCAR or ERA40 reanalysis, these long-term reanalysis have the advantage that upper-air datasets coming from satellites were not assimilated, which makes them more homogeneous in terms of the type of assimilated observations. However, their early-century homogeneity is still questioned due to too few observations in some areas. Wang et al. (2013) used 6-hourly MSLP from the 56 members of 20CR between 1871 and 2010 to obtain NH tracked-cyclones information for all seasons. They obtained an increase in intense cyclones and a poleward shift of the storm tracks for the entire century. They also showed that the ATL and European regions are the most statistically homogeneous regions for cyclone statistics since 1871.

Wang et al. (2016) compared eight reanalyses with different resolution and temporal ranges and applied the same tracking algorithm on unfiltered MSLP data for all the seasons. They found important differences in trends due to data resolution. Reanalyses covering recent decades show good agreement, particularly from the beginning of satellite-data assimilation in 1979. For the two long-term reanalysis they found ERA-20C to be more homogeneous than 20CR (specially in the Arctic) and better correlated with other shorter reanalyses. However, both reanalyses show inhomogeneities in the beginning of the century and in the Southern Hemisphere. Regarding cyclones trends, both reanalyses show an increase in deep cyclones over the NH for the 20th century period. However, as shown by several authors, the origin of inconsistencies of observed trends in long-term reanalyses is still on open question. They emphasized that the variation of observations density along the century must be assessed (Krueger et al. 2013; Wang et al. 2016; Chang and Yau 2016). For example, Dell'Aquila et al. (2016) show questionable lower synoptic activity in the early decades of ERA-20C and 20CR.

Finally, Chang and Yau (2016) applied a tracking algorithm to SLP data for the winter months (DJF) using several reanalyses including the two long-term reanalysis and have also computed the 300-hPa meridional wind variance. In general, results for the period 1960–2010 show positive trends in cyclones in ATL and a greater increase in PAC. It confirms previous studies, especially that of Chang and Fu (2003) who showed, following a mean-flow-based proxy,

that storm-track activity was weakest during 1960s and then underwent an upward trend until 1990s.

The present paper aims at investigating temporal trends of moderate-deep winter cyclones using ERA-20C. While Wang et al. (2016) and Chang and Yau (2016) used MSLP tracking algorithms, extratropical cyclones are here detected with a vorticity-based algorithm. Besides, the main originality of the paper relies on the physical interpretation of the detected cyclone trends in terms of barolinicity trends and changes in phase of large-scale modes of climate variability. The results become more robust when a dynamical link between cyclone trends and the large-scale circulation is found. This also helps eliminating some doubts associated with the inhomogeneity of the reanalysis.

There is also a growing literature investigating the evolution of storm tracks and jet stream in a changing climate. A poleward shift of the Atlantic and Pacific storm tracks occurred after the 80s until the end of the 90s (McCabe et al. 2001; Wang et al. 2006) in connection with a tendency toward a positive phase in the North Atlantic Oscillation (NAO) and Arctic Oscillation (AO) indices (McCabe et al. 2001). This has been initially attributed to the anthropogenic forcing (Thompson and Wallace 1998; Corti et al. 1999). However, since the early 2000s, the poleward tendency disappeared and some winters were marked by extreme negative NAO and AO (LHeureux et al. 2010; Cattiaux et al. 2010; Rivière and Drouard 2015). There is thus no general shift of the jet streams or storm tracks in the last decades in the Northern Hemisphere but rather regional shifts (Barton and Ellis 2009). Besides, the variations of the recent decades do not appear unusual (Woollings et al. 2014) and could be due to internal atmospheric variability (Barnes and Screen 2015). Nor is there a strong signal in the future evolution of the Northern Hemisphere storm tracks and jet streams in winter as seen in climate model projections of the Coupled Model Intercomparison Project (CMIP) (Cattiaux and Cassou 2013). Depending on model properties, such as resolution, ocean or sea-ice dynamics, the results can change significantly (Woollings et al. 2012). However, despite a large spread of CMIP5 models, there are some agreements about storm-track changes in the NH: a slight upward and poleward shift in the upper troposphere in both seasons and an overall decrease in the lower troposphere except in some specific regions like an eastward extension of the wintertime storm track over Northern Europe (Chang et al. 2012; Harvey et al. 2013; Zappa et al. 2013).

Mid-latitude cyclone activity strongly depends on baroclinicity, a large-scale atmospheric quantity function of horizontal and vertical temperature gradients (Hoskins and Valdes 1990; Geng and Sugi 2003). The recent strong increase in the Arctic temperature tends to reduce the near-surface meridional temperature gradient and so, the lower-level baroclinicity. The effect is to decrease storm-track activity and displace the jet streams equatorward according to idealized experiments (Butler et al. 2010; Rivière 2011). Consistently, more realistic simulations show that sea-ice reduction favours the occurrence of the negative AO/NAO patterns (Bader et al. 2011; Cohen et al. 2014; Nakamura et al. 2015; Oudar et al. 2016). However, in the upper troposphere, the mid-latitude temperature gradients increase due to a stronger warming in the tropical upper troposphere which counteracts the effect of the decrease in lower-level baroclinicity and acts to shift the storm tracks poleward (Butler et al. 2010; Rivière 2011). These opposing effects of changes in lower- and upper-level baroclinicity participate in keeping the future evolution of the wintertime NH storm tracks uncertain (Shaw et al. 2016). Nevertheless, some consensual results seem to appear with the last multi-model intercomparison studies using cyclone tracking algorithms. We expect an overall decrease in strong winter cyclones and, in the North Atlantic sector, an increase in cyclone frequency near the British Isles (Chang et al. 2012; Zappa et al. 2013). These CMIP5 experiments confirm previous studies relying on single model experiments (Bengtsson et al. 2006; Pinto et al. 2007; McDonald 2010). Even though the present study does not investigate future changes in storm-track activity, the question of the effect of Arctic warming on mid-latitudes will be put in perspective with the earlier periods of the 20th century.

Since the present paper focuses on cyclone variability over more than a century, multi-decadal fluctuations could be detected in connection with well-known modes of ocean (multi-)decadal variability like the Atlantic Multidecadal Oscillation (AMO) and Pacific Decadal Oscilation (PDO). In the Pacific, the PDO is positively correlated with storm tracks until the 80s and its negative (positive) phase is associated with a northward (southward) shift of the Pacific storm track (Lee et al. 2012; Sung et al. 2014). In the Atlantic, the negative AMO phase is related with more zonal and elongated storm tracks (Yamamoto and Palter 2016). A warm AMO has been shown to lead to a negative NAO by a few years (Peings and Magnusdottir 2014; Gastineau and Frankignoul 2015). The AMOC circulation has weakened since the middle of the century and future scenarios predict a constant decrease (Rahmstorf et al. 2015). Its weakening and/or shutdown means less exchange between warm tropical and cool polar waters, an increase in the SST gradients and low-level baroclinicity which leads to an increase in the intensity of the Atlantic storm-tracks, consistent with the Bjerknes compensation mechanism (Shaffrey and Sutton 2006). A more recent study has shown that the dynamical link between the NAO and deep cyclones is modulated by the variability of the AMOC (Gomara et al. 2016).

The present paper is organized as follows. Data and methods are described in Sect. 2. In Sect. 3, moderate to strong extratropical cyclone variability in the NH are first presented and trends for some periods of the 20th century

are identified. A comparison with trends in high-frequency kinetic energy is also made. In Sect. 4, baroclinicity and baroclinic conversion trends that may explain the detected cyclone trends are identified and interpreted in terms of changes in temperature and zonal wind for three different periods. Section 5 makes the link between changes in phase of large-scale modes of atmospheric and oceanic variability and baroclinicity changes. The potential impact of nonhomogeneous assimilated observations is discussed in Sect. 6. Finally, a summary of the results is provided in Sect. 7 and are discussed relative to the existing literature.

2 Data and methodology

2.1 Data

The data used in this study is the ECMWF ERA-20C reanalysis that covers the whole 20th century (Poli et al. 2016). The focus is made on the Northern Hemisphere (0°–90°N; 180°W–180°E) during the cold season (October–March) from 1900 until 2010. Datasets were extracted with a 3-hourly frequency as needed to feed the cyclone tracking algorithm. It concerns the relative vorticity at 850 hPa and the horizontal wind components at 700 and 850 hPa. We extracted the wind and temperature at five vertical levels (850/700/500/300/200 hPa) at a daily frequency as well as the 2-meter temperature, sea surface temperature (SST) and surface pressure. All data was extracted with a spatial resolution of $1.125° \times 1.125°$.

2.2 Cyclone tracking algorithm

The tracking algorithm used is the one from Ayrault (1998) and Ayrault and Joly (2000) (see also the supplementary material of Michel et al. 2012 for a description of a recent climatology in the North Atlantic). It has been adapted to track 3-hourly relative vorticity maxima at 850 hPa over the entire Northern Hemisphere. A spatial smoothing distance-weighted filter is applied to the relative vorticity at each grid point with respect to its 13 closest neighbours. The tracks are built by pairing successive relative vorticity maxima following several criteria: Two maxima are paired when they present similarity in intensity, and if the displacement between them is coherent with the advection by the background wind as determined by both winds at 700 and 850 hPa. Final trajectories were selected only if the duration of life and travelled distance were superior to 24 h and 600 km respectively. The tracking period runs between the 1st of October to the 31rd of March from 1900 to 2010. Even though the tracking algorithm detects all vorticity maxima, only trajectories whose relative vorticity exceeds 10^{-4} s^{-1}, that is roughly the value of the Coriolis parameter, are kept

in the present paper. It means that only moderate to deep cyclones are hereafter considered. The main reason is that such a vorticity-based cyclone tracking algorithm detects small-scale features with relatively weak vorticity values that are not necessarily detected by other tracking algorithms based on geopotential or mean sea level pressure.

2.3 Baroclinicity

In this paper, we compute the baroclinicity and baroclinic conversion as follows:

$$\sigma_{BC} = \frac{1}{\sqrt{S}} \sqrt{\left(\frac{\partial \overline{\theta}}{\partial x}\right)^2 + \left(\frac{\partial \overline{\theta}}{\partial y}\right)^2}, \tag{1}$$

$$BC = -\frac{1}{S}\frac{\partial \overline{\theta}}{\partial y}\overline{\theta' v'} + \frac{1}{S}\frac{\partial \overline{\theta}}{\partial x}\overline{\theta' u'}, \tag{2}$$

where overbar and prime quantities represent the mean flow and eddy fields respectively. The stratification parameter $S = -\frac{p}{R}\left(\frac{p}{p_0}\right)^{-\frac{R}{C_p}}\frac{\partial \theta_R}{\partial p}$ considers a reference potential temperature θ_R which is a priori a function of the pressure only. Variables p and p_0 indicate the pressure and the reference pressure respectively, R and C_p are the gas constant for the air and the specific heat at constant pressure The parameter σ_{BC} corresponds to the maximum baroclinic exponential generation rate, that is the maximum of the ratio between the baroclinic conversion and the eddy total energy (Rivière et al. 2004; Rivière and Joly 2006). In the whole paper, the mean flow and eddy fields correspond to the seasonal mean (October–March) and high-pass-filtered (periods less than 10 days) fields respectively and the reference potential temperature θ_R is taken as the annual mean of θ (i.e $\overline{\theta}$). Finite differences between 200–300, 200–500, 300–700, 500–850 and 700–850 hPa are applied to the potential temperature to compute the stratification parameter at 200, 300, 500, 700 and 850 hPa respectively. Grid points for which the surface pressure is lower than 850 hPa are suppressed from the computation. Note finally that σ_{BC} is just the Eady parameter divided by the constant coefficient 0.31 (Hoskins and Valdes 1990).

2.4 Climate modes of variability

Regarding planetary modes of variability we computed the Atlantic Multidecadal Oscillation (AMO) and Pacific Decadal Oscillation (PDO). The AMO was computed from monthly (October–March) SST anomalies in the North Atlantic (90°W–30°W; 0°N–70°N) that are first detrended and then smoothed with an approximative 120-month running mean (Enfield et al. 2001). The PDO (Mantua et al.

1997) was computed as the first EOF of monthly SST anomalies between 20°N and 90°N in the North Pacific also for the October–March months.

2.5 Trends and statistical significance

Finally, all trends were computed with a robust linear, non-parametric Kendall–Theil trend estimator (Theil 1950), that computes all possible pairwise slopes and takes the median as the summary statistic that describes the trend. We considered a 5% significance level.

3 Extratropical cyclone and storm-track trends

3.1 Cyclone frequency trends

Extratropical cyclones (ETCs) tracks are separated into three categories according to the maximum vorticity intensity. In the whole study, only trajectories with maximum vorticity greater than or equal to the Coriolis parameter ($f_0 = 10^{-4} s^{-1}$) are considered (hereafter referred to as *All*), which is around 45% of the total number of trajectories. Then, the ones from *All* that never reach its percentile 85 ($2.13 \times 10^{-4} s^{-1}$) are labelled as *Moderate* and finally the ones that have reached maximum vorticity greater than this value are labelled as *Strong*.

Figure 1a presents the normalized number of cyclones per year in the Northern Hemisphere (here defined as the area 20°–90°N; 180°W 180°E) for *All* (black), *Moderate* (blue)
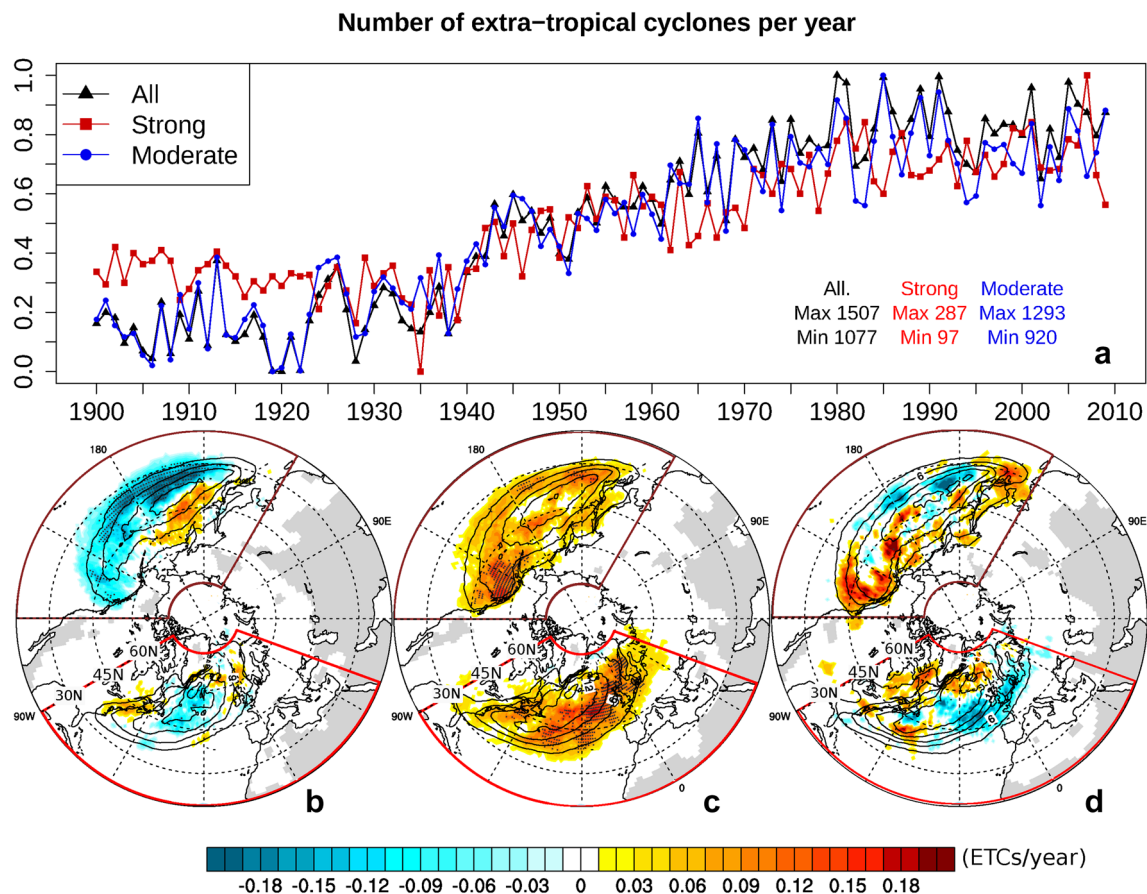
Fig. 1 a Time evolution of the number of ETCs with maximum vorticity higher than f_0 for all storms (black line), Strong (red line) and Moderate (blue line). Each number has been first subtracted by the minimum before being divided by the range. Trends in the number of strong ETCs per year are shown for different periods: **b** 1900–1935, **c** 1935-1980 and **d** 1980–2009. The red and brown areas on **b**–**d** represent the Atlantic and Pacific sectors respectively as defined in the study. Contours lines represent the mean number of strong ETCs per year for each period (contour intervals three cyclones per year). Dotted grid points represent significant values with a minimum 95% confidence

and *Strong* (red) ETCs. The normalization is obtained by subtracting the absolute minimum to the number of cyclones per year and then dividing the result by the range over the total period. Three time periods can be distinguished: one period at the middle of the century with a positive trend and two periods at the beginning and at the end of the century that undergo rather small variations in cyclone frequency. The first period goes from 1900 to 1935 and is marked by a very slight decrease in *Strong* cyclones and almost no change in *All* cyclones. The second period from 1935 to 1980 is characterized by an increase in all categories of ETCs and the third period from 1980 to 2010 by almost no change in the number of cyclones. The three periods are hereafter denoted as periods I, II and III. Besides these previously defined three periods, we also consider two different regions: the ATL region (20°–90°N; 90°W–60°E) and the PAC region (20°N–90°N; 120°E -120°W) defined by red and brown polygons in Fig. 1b–d.

We compute ETC density trends (as described in Sect. 2) for these three periods. Trends and related significances are summarised in Table 1. Considering the whole century (Table 1 first column), significant positive trends are observed for all regions and all types of ETCs. The numbers of *All* and *Strong* ETCs increase during the century from 1.5 to 3 times (Fig. 1a). The increased number of ETCs during the century essentially occurs during the second period (1935–1980). PAC and ATL show similar positive trends for this period as for the whole 20th century (Table 1 third column). The *All* ETCs are the ones with higher positive trends while the *Strong* are the ones that show the weakest positive trends. The first period does not present significant trends except for the *All* ETCs in ATL and *Moderate* in PAC (Table 1 second column). The third period does not show any significant trend for any type of ETCs and any region (Table 1 fourth column).

Figure 1b–d present spatial trends in the number of *Strong* ETCs for the three previously defined time periods

Table 1 Trends in the number of ETCs per year and regions for the three different periods studied

		1900–2010	1900–1935	1935–1980	1980–2010
	All	1.3**	0.77*	2**	–
ATL	Strong	0.40**	–	0.786**	–
	Moderate	0.90**	–	1.2**	–
	All	1.12**	–	2**	–
PAC	Strong	0.25**	–	0.577**	–
	Moderate	0.86**	0.69*	1.492**	–
	All	3.69**	–	5.35**	–
NH	Strong	0.95**	−0.515**	1.524**	–
	Moderate	2.72**	1.3*	3.75**	–

*p value lower than 0.15, **p value lower than 0.01

in the Northern Hemisphere. The first period is characterized by significant negative trends in the southernmost latitudes of the PAC storm track and positive trends on the northwestern part of the storm track. There is a poleward shift of the storm track accompanied by some reduced intensity overall. As suggested by the time series of Fig. 1a, the second period shows significant positive trends in both the Pacific and Atlantic storm-track regions, especially on their eastern sides. The third period shows weak and non-significant trends. We note however some increase in storm frequency in the eastern Pacific and some decrease in the eastern Atlantic.
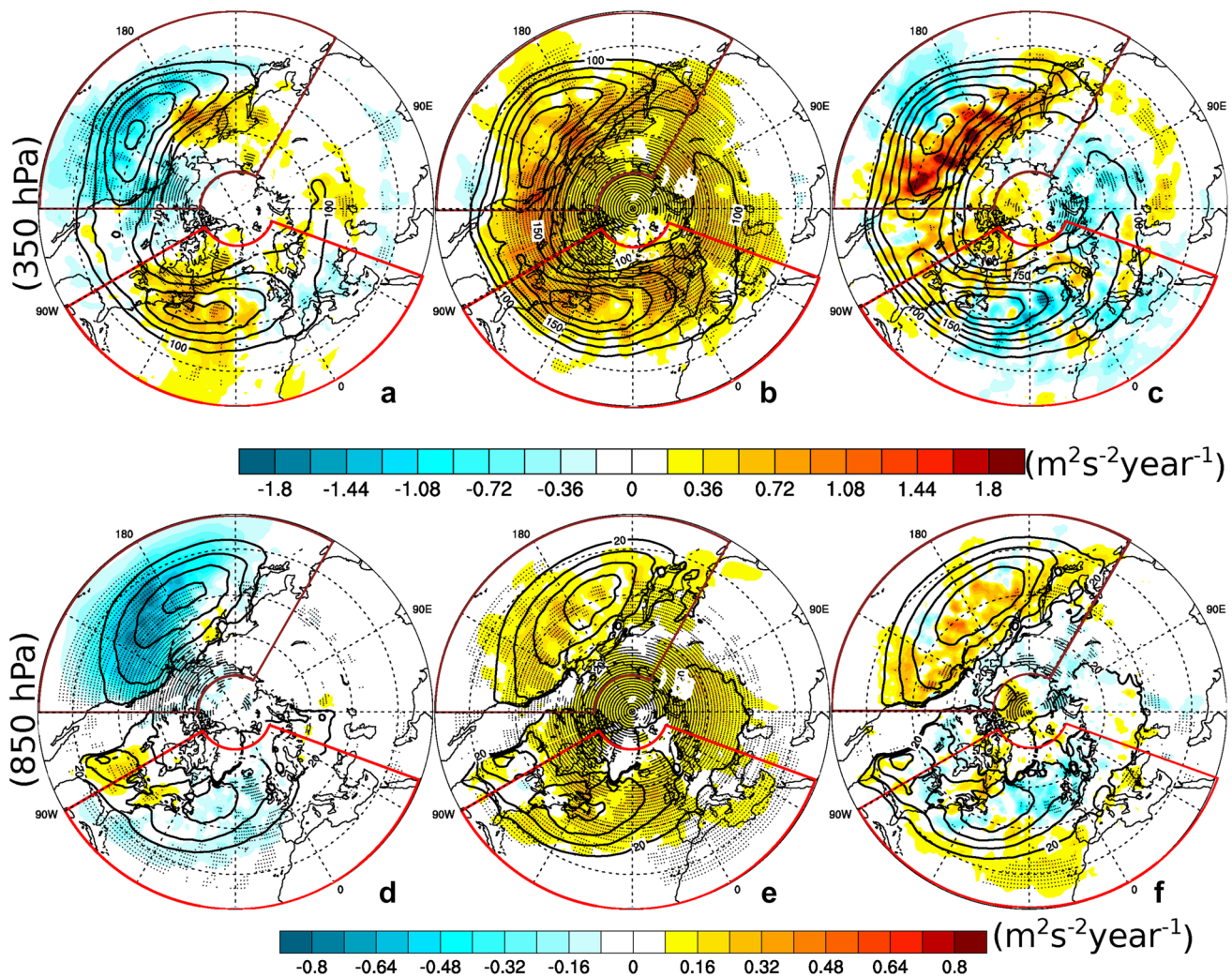
3.2 High-frequency eddy kinetic energy trends

Figure 2 displays spatial trends of high-frequency eddy kinetic energy at 300 and 850 hPa. For the first period (Fig. 2a, d), negative trends can be found over the southern and eastern regions of the PAC storm track and positive trends in the northwestern regions at upper levels in particular. In the Atlantic sector, upper and lower levels behave differently with positive and negative trends respectively, except for the east coast of the US which is characterized by an increase at the two different levels, similarly to the number of ETCs (Fig. 1b). For the second period, positive trends are observed over the entire NH at both levels, consistent with the positive trends found in the number of ETCs (Fig. 1a–c). The third period is less characterized by broad areas of significant patterns but rather by small regional changes such as the increase in the northeastern PAC storm-track and decrease in the eastern ATL storm-track. Therefore Figures 1 and 2 show that ERA-20C tracking and high-frequency variance trends are in good agreement regarding the most remarkable features of each period.

Another important feature to notice is that *Strong* ETCs trends are located in the storm-track regions, i.e, over the oceans while *Moderate* trend maximums are also significant over the continents (not shown). This is important because we know that the number of observations assimilated by the reanalysis explodes between the 40s and the 60s over the continents [Fig. 3 from Poli et al. (2016)] while over the oceans the number of assimilated observations is more homogeneous since the beginning of the century (especially over the ATL). Though we are not able to fully address the sensitivity of the storm-track trends to the observation density trends it suggests that *Strong* ETCs trends should be more reliable that *Moderate* ones. Moreover, no decrease in the yearly number of ETCs (Fig. 1) is observed during world war I and II, when the number of observations has dramatically reduced (Fig. 4, Poli et al. 2016). For all the

Fig. 2 Spatial trends in high-frequency eddy kinetic energy (shadings; units: m²s⁻²year⁻¹) at **a–c** 300 hPa and **d–f** 850 hPa for (left column) 1900–1935, (middle column) 1935–1980 and (right column) 1980–2009. The black contours represent the mean field for each subperiod (interval: 25 m²s² for **a–c** and 10 m²s² for **d–f**). Dotted grid points represent significant values with a minimum 95% confidence

aforementioned reasons we decide to focus on the *Strong* ETCs trends only.

3.3 Extreme winds trends

Most of the strong ETCs crossing the Atlantic have a strong impact over Europe. For this reason, extreme winds in the Europe can be used as an indicator of storm intensity. Figure 3 confirms the intensification of extreme ETCs during the 1935–1980 period in the European sector as diagnosed from the 98% percentile of the 10-m wind speed. Before 1935, the yearly 98% percentile is systematically below 11 m s⁻¹. Then, it smoothly increases until the 1980s where it reaches values near 11.4 m s⁻¹. After the 1980s, it slight decreases. It is an important confirmation of the above results using a very different variable.

The rest of the paper is dedicated to exploring the reliability of the previously detected density trends. For that purpose, we compute planetary-scale diagnoses relevant to mid-latitude storm-track dynamics and less sensitive to analysis quality. Section 4 presents the baroclinicity trends as diagnosed for each subperiod, together with the baroclinic conversion, temperature and zonal-mean zonal wind trends.
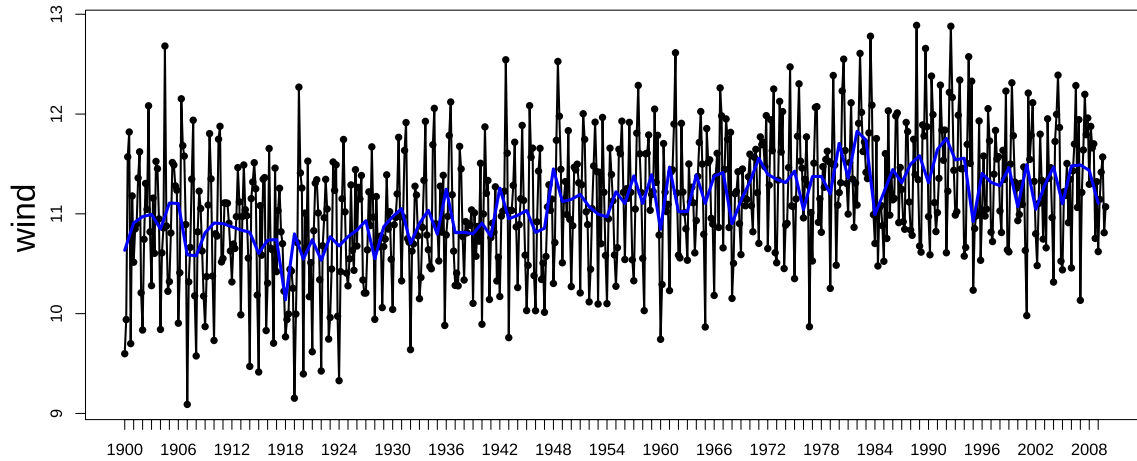
4 Baroclinicity trends
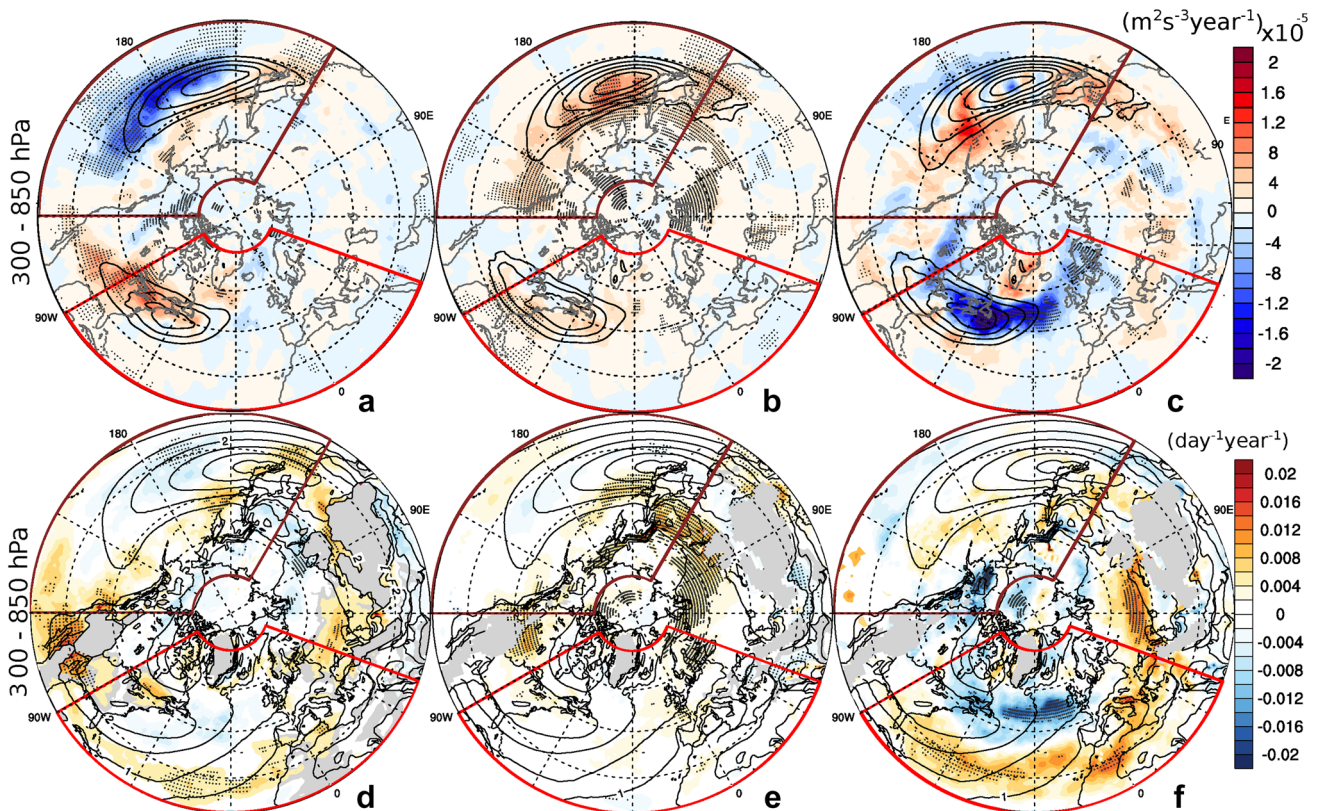
4.1 Period I: 1900–1935

For the first period, the PAC region shows weak positive and strong negative tendencies of baroclinic conversion

Mean European 98 percentil of the Wind

Fig. 3 Monthly (black) and yearly (blue) time series of the mean 98th percentile of 10-m wind speed (units: m s^{-1}) in ERA-20C averaged in the European regions (34°W–30°E, 35°N–75°N)


Fig. 4 Same as Fig. 2 but for the vertical average between 300 and 850 hPa of **a**–**c** baroclinic conversion (m^{2}s^{-2}year^{-1}) and **d**–**f** baroclinicity (day^{-1}year^{-1}). The black contours represent the mean field for each period (interval: 25 m^{2}s^{-2} for the baroclinic conversion and 0.5 day^{-1} for the baroclinicity). Dotted grid points represent significant values with a minimum 95% confidence

at northern and southern latitudes respectively (Fig. 4a) leading to an overall decrease and a slight poleward shift of the conversion pattern. These trends are consistent with the storm-track ones. The vertically-averaged baroclinicity also exhibits a poleward shift (Fig. 4d) and the decrease on the equatorward side is more pronounced than that on the
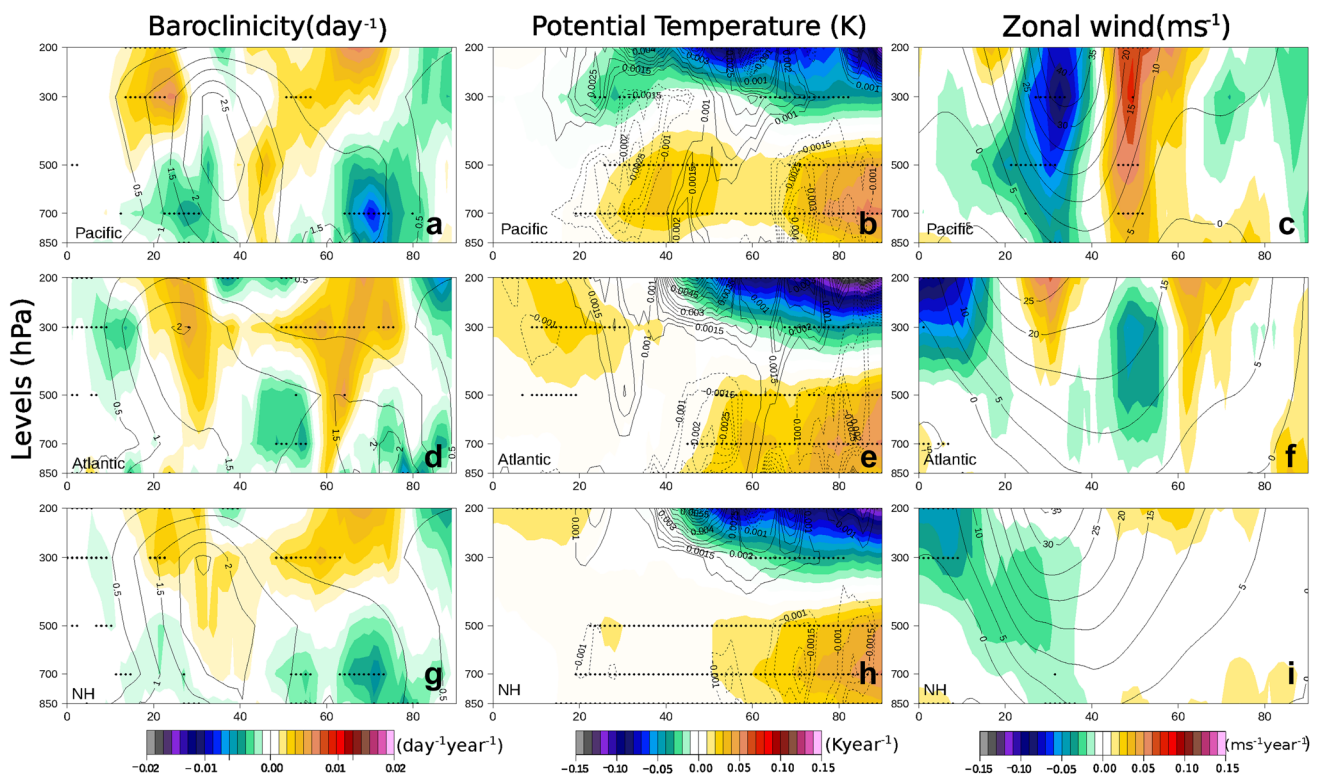
Fig. 5 Vertical profiles for period I (1900–1935) of (first column) the baroclinicity trends (colors, day^{-1}year^{-1}) and the mean field (contour); (second column) potential temperature trends (colors, Kyear^{-1}) and temperature gradient trends (positive and negative values in solid and dotted contours); (third column) Zonal wind trends (colors, ms^{-1}year^{-1}) and mean field (contours; int: 5 ms^{-1}). (top) Pacific, (middle) Atlantic and (bottom) Northern Hemisphere

poleward side in the lower troposphere as seen in Fig. 5a. There is also some decrease in the baroclinic conversion in the polar regions near Alaska which can be explained by a decrease in baroclinicity there (Figs. 4a, d, 5a). However, this should have no impact on the ETCs since it occurs over a region of weak baroclinicity. The baroclinicity trends are well correlated with horizontal temperature gradient trends (Fig. 5b). The poleward shift of the mid-latitude baroclinicity is due to a warming centred near 40°N and the decrease in baroclinicity north of 60°N is due to a stronger warming in the polar cap regions. Finally, westerlies decrease in intensity and are slightly poleward shifted (Fig. 5c) similarly to the Pacific storm-track.

In the ATL region, positive tendencies of the baroclinicity are observed at the entrance of the ATL storm-track (Fig. 4d), an area where the baroclinic conversion tendency is also significantly positive (Fig. 4a). More downstream in the mid-Atlantic, the baroclinicity tendencies are weakly negative and not significative which might be due to the compensation between the negative tendencies at low levels and the positive ones at upper levels (see the vertical cross-section of Fig. 5d). There is some increase in baroclinicity in the subtropical North Atlantic near 30°N (Fig. 4d) which mainly comes from the warming of the upper-level tropical

troposphere (Fig. 5d,e). Generally speaking, baroclinicity changes are well captured by horizontal temperature gradient changes. Thus, its decrease in intensity at low levels is explained by the warming of the polar regions below 500 hPa (Fig. 5e). Westerlies generally decrease even though the anomalies are not significative (Fig. 5f).

Northern Hemisphere tendencies (Fig. 5g–i) are much smoother than PAC and ATL ones, since we observe opposite trends for the ATL and PAC regions at many latitudes. The general tendency is a polar warming confined to the lower troposphere that reaches a peak amplitude in the mid-1930s as described in Polyakov and Johnson (2000) and Yamanouchi (2011). The polar warming leads to the decrease in the lower-troposphere baroclinicity. But because the upper-level baroclinicity increases during that period, there is some compensation that may explain why the decrease in storm-track eddy activity is not significant.

4.2 Period II: 1935–1980

For the second period, in the PAC region, baroclinic conversion trends are positive and significant everywhere (Fig. 4b) with a maximum trend reached in the western Pacific where the mean baroclinic conversion is the strongest. This

maximum positive trend is closely related to the area of positive baroclinicity trend northeast of Japan (Fig. 4e). There are also other areas of increased baroclinicity and baroclinic conversion over the continents in Eastern Asia and over the west coast of North America. Zonal averages of the baroclinicity confirms a global increase in baroclinicity in the PAC sector at almost all tropospheric levels between 40°N and 80°N (Fig. 6a). There is just a moderate decrease in baroclinicity on its equatorward flank at low levels near 35°N. The overall baroclinicity increase north of 40°N is due to a cooling at high latitudes (Fig. 6b). The Pacific jet tends to widen with a stronger increase on its poleward flank (Fig. 6c).

In the ATL region, baroclinic conversion trends are also positive and significant in the western Atlantic but amplitudes of the trends are weaker than in the PAC region (Fig. 4b). The vertically-averaged baroclinicity in the ATL sector is weakly positive and not significant and the strongest positive trends are reached over land in the eastern North America and near Scandinavia. Cross-section of Fig. 6d confirms the slight positive trend but the number of significant grid points is smaller than in the PAC sector. Positive significant values north of 60°N at low levels are related with the positive values over the Scandinavian region. The general positive baroclinicity trend can be attributed, as in the PAC sector, to an increase in horizontal temperature gradients

due to a cooling at high latitudes over the whole troposphere (Fig. 6e). The ATL jet also intensifies on its poleward flank during that period (Fig. 6f), consistent with the observed cooling.

In the NH, the zonally-averaged tendencies of Fig. 6g–i are quite significant because the PAC and ATL regions undergo more or less the same changes. There is an overall increase in baroclinicity which is more important north of its maximum amplitude (Fig. 6g) due to a general cooling at high latitudes (Fig. 6g, h) as observed by Box et al. (2009) and Kinnard et al. (2008). This is accompanied by an intensification of the westerly jets on their poleward flank (Fig. 6i). The baroclinicity intensification, especially on the northernmost latitudes, explains why there is a global increase in storm-track eddy activity and in the number of moderate and strong ETCs during that period. Further and more detailed analysis for this period is presented on Sect. 5.

4.3 Period III: 1980–2009

Period III shares common features with period I though important differences can be depicted. In the PAC region, both the baroclinic conversion and baroclinicity show positive consistent trends (Fig. 4c, f), accompanied by a northeastward shift (Figs. 4c, f, 7a) similarly to period I. The baroclinicity decrease north of 60°N mainly occurs over
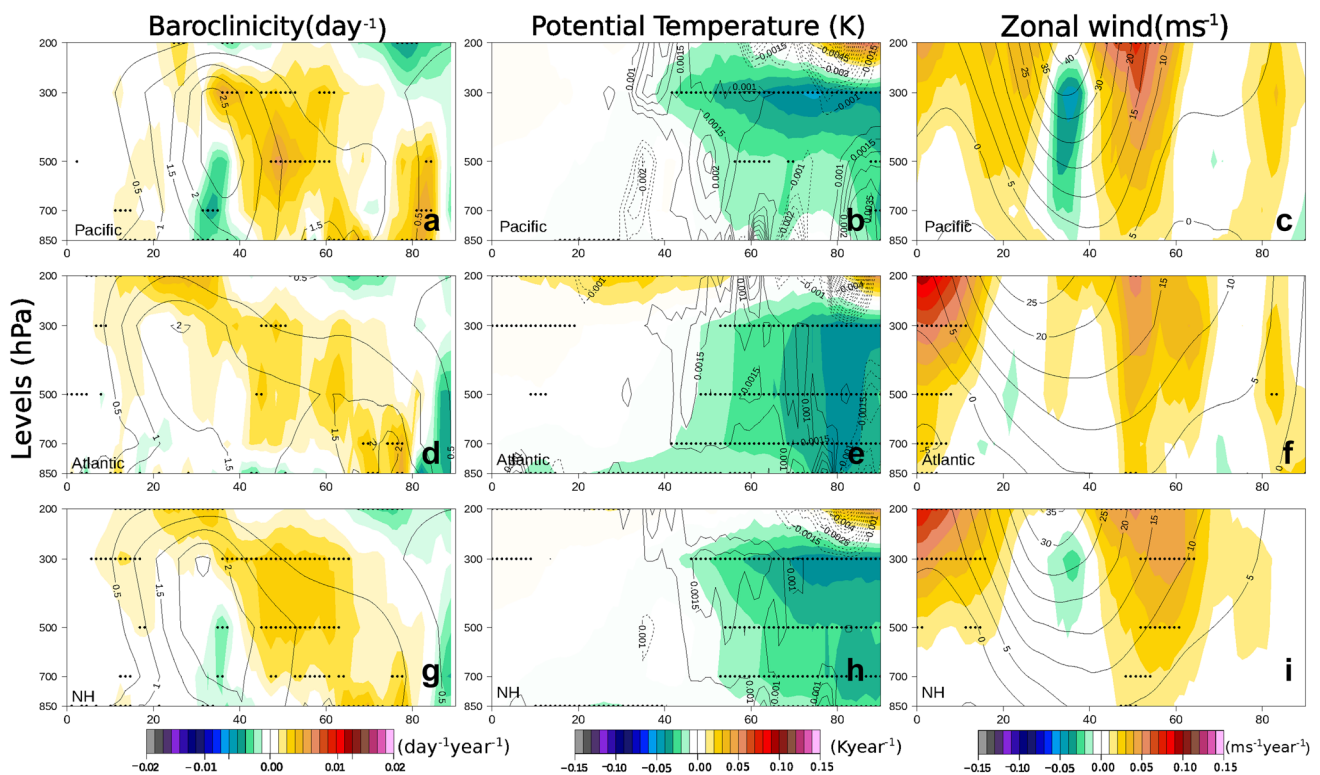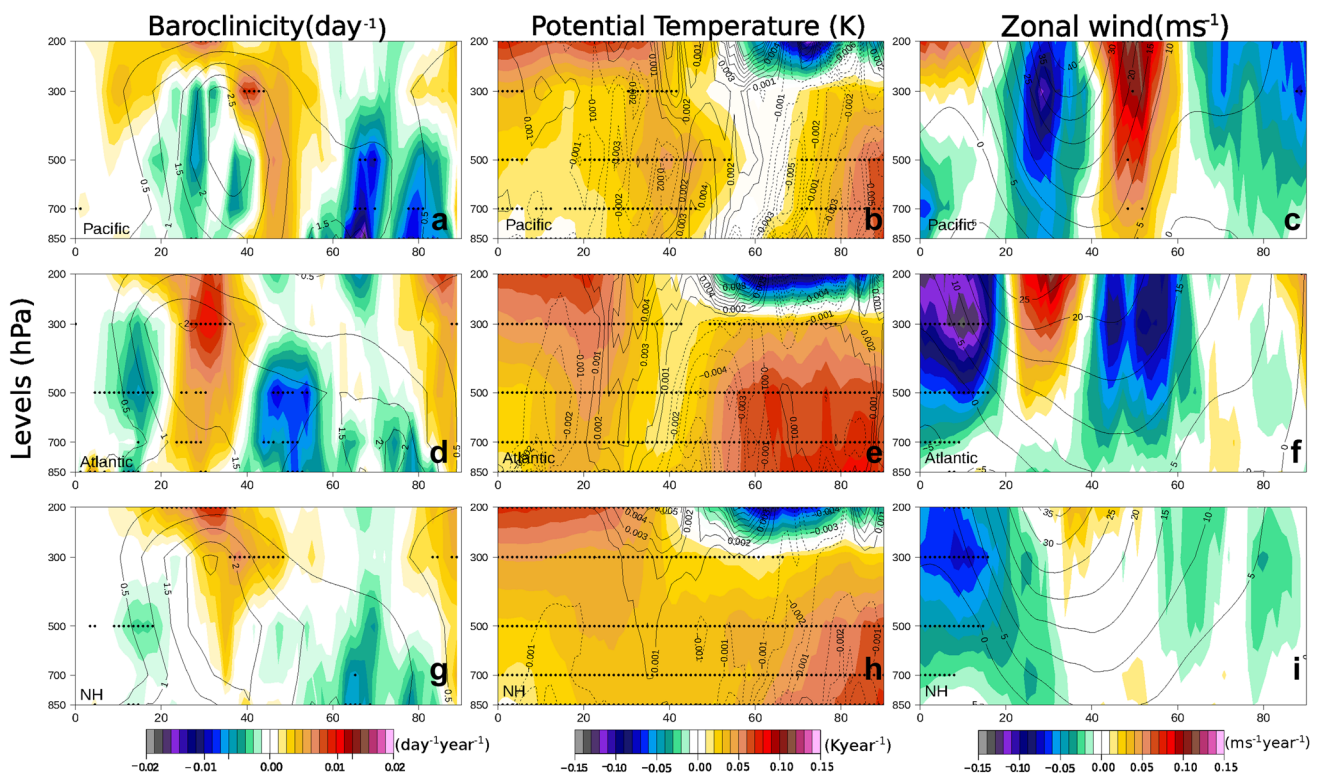

Fig. 6 Same as Fig. 5 but for period II (1935–1980)

Fig. 7 Same as Fig. 5 but for period III (1980–2010)

Alaska but in a region of weak mean baroclinicity and small-amplitude eddies and this should not affect the storm-track. The poleward-shifted baroclinicity near 40°N is mainly due to a warming there (Fig. 7b) and provides an explanation for the north-eastward shift of the storm-track related parameters (Figs. 1d, 2c, f). There is consistently a clear poleward shift of the westerlies. This is coherent with an increase in intensity of the PAC jet stream at the same location observed by Barton and Ellis (2009).

In the ATL region, nevertheless, significant negative tendencies exist at mid latitudes for both the baroclinic conversion and the baroclinicity (Figs. 4c, f, 7d), while positive trends are observed further north and south of the storm-track latitudes, mostly for the baroclinicity. Temperature profiles show the occurrence of a tropical upper-level warming together with a polar lower-level warming (Fig. 7e) that do impact the baroclinicity and the position and strength of the jet and the storm-track. The tropical upper-level warming induces a baroclinicity increase near 30°N while the high-latitude lower-level warming decreases the baroclinicity in storm-track latitudes. The latter decrease probably explains the diminished storm-track eddy activity in the eastern North Atlantic (Figs. 1d, 2c, f). The eddy-driven jet located between 40°N and 60°N is also decreasing in intensity because of the weakening of the storm track (Fig. 7i).

As in period I, the PAC and ATL tendencies largely compensate each other and the NH tendencies are rather weak (Fig. 7g–i). But the positive temperature trends are more intense, extend more to upper levels and cover more southernmost latitudes than in period I.

4.4 Synthesis

The following section presents a synthesis of the previous results. Figure 8 presents the time evolution of the Northern Hemisphere yearly-mean baroclinicity at different levels together with the vertical average. Linear trends are computed and highlighted (solid straight lines) when significant. For period I, the upper-level baroclinicity has a significant positive trend (red line in Fig. 8), while the low-level baroclinicity (at 850 and 700 hPa) shows significant negative tendencies (green and orange lines of Fig. 8). The vertically-averaged baroclinicity does not present any significant trend. For period II, the yearly-mean baroclinicity increases and has significant positive trends for all levels (except at 850 hPa), including the vertically-averaged baroclinicity (black line in Fig. 8). Finally, during period III, the baroclinicity increases at upper levels and decreases at lower levels, similar to period I.

Figure 9a shows the time evolution of normalized values of yearly (dashed lines) and 11-year running mean (solid

Fig. 8 Time evolution of the Northern Hemisphere baroclinicity (units: day⁻¹) for various vertical levels (color) and the vertical average between 300 and 850 hPa (black)
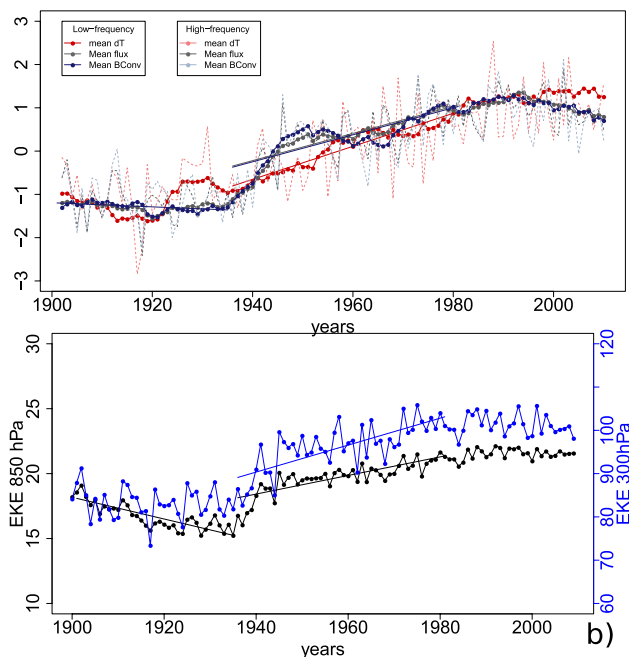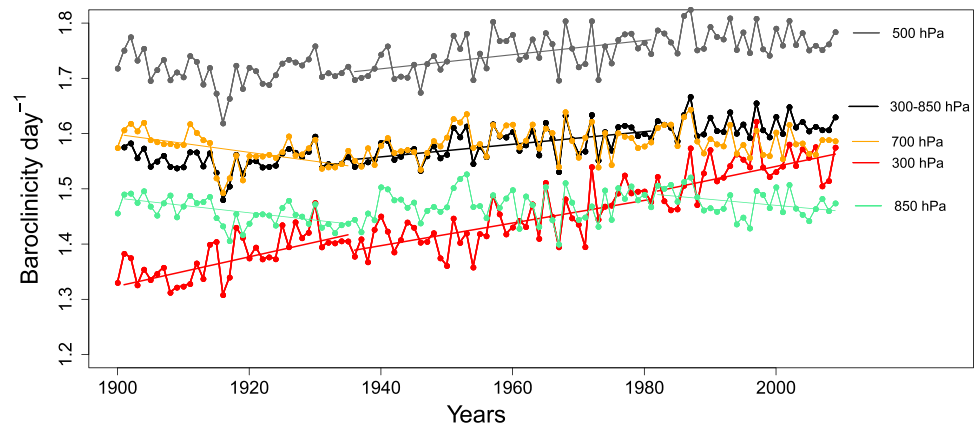
Fig. 9 Top: Northern Hemisphere scaled values of yearly (dashed-blue) and 11-years run-mean (blue) of baroclinic conversion, yearly (dashed-red) and 11-years run-mean (red) modulus of the horizontal gradient of temperature, yearly (dashed-grey) and 11-years run-mean (grey) modulus of the horizontal mean heat fluxes. Bottom: yearly-mean eddy kinetic energy at 850 hPa (black) and 300 hPa (blue) in the Northern Hemisphere

lines) of the vertical-averaged baroclinic conversion (blue) and its two main components, the magnitude horizontal heat fluxes ($1/\sqrt{S}\sqrt{\overline{\theta'u'}^2 + \overline{\theta'v'}^2}$) in grey and baroclinicity in red (σ_{BC}, Eq. 1).

All parameters show a general positive trend from the 40s up to late 80s However, the baroclinic conversion (black lines of Fig. 9a) is more in phase with the magnitude of the heat fluxes (grey lines of Fig. 9a) than with the baroclinicity (red lines of Fig. 9a). During period II, all the three parameters

present significant positive trends together with the eddy kinetic energy at lower and upper levels (Fig. 9b). Period I is marked by significant negative trends for the baroclinic conversion and the lower-level eddy kinetic energy but not for the other parameters of Fig. 9. A particular rapid increase between late 30s and early 40s is visible for all the variables that include quadratic measures of the high-frequency eddies (eddy heat fluxes, eddy kinetic energy and baroclinic conversion) but this is much less visible for the baroclinicity. A deeper analysis show that this rapid increase in eddy-related fields happens in the PAC region and is accompanied by a rapid increase in horizontal temperature gradient though a much less rapid increase in baroclinicity due to the negative trend in the stratification parameter in presence of a strong cooling in the high latitudes near the surface (see supplementary material). To conclude, systematic and significant positive trends are found during period II for all variables measuring the intensity of eddy activity. It is consistently accompanied by a global increase in baroclincity even though some disagreements between the eddy-related parameters and the baroclinicity may appear during specific shorter periods. The purpose of next section is to interpret these changes in baroclinicity and baroclinic conversion especially by looking at the ocean multi-decadal variability.

5 Link with ocean variability

Since significant multi-decadal variability is found in the reanalyses, the role of the ocean variability must be questioned. The AMO index (red line in Fig. 11a) is negative during the beginning of the century and becomes positive at the end of period I, being consistent with SST positive trends during period I (Fig. 10b). Between 1930 and 1950, AMO stays in its warm phase and rapidly shifts to a cold phase between 1960 and 1975, in agreement also with SST negative trends observed in Fig. 10c. After the 90's, SST trends become again strong and positive, showing an
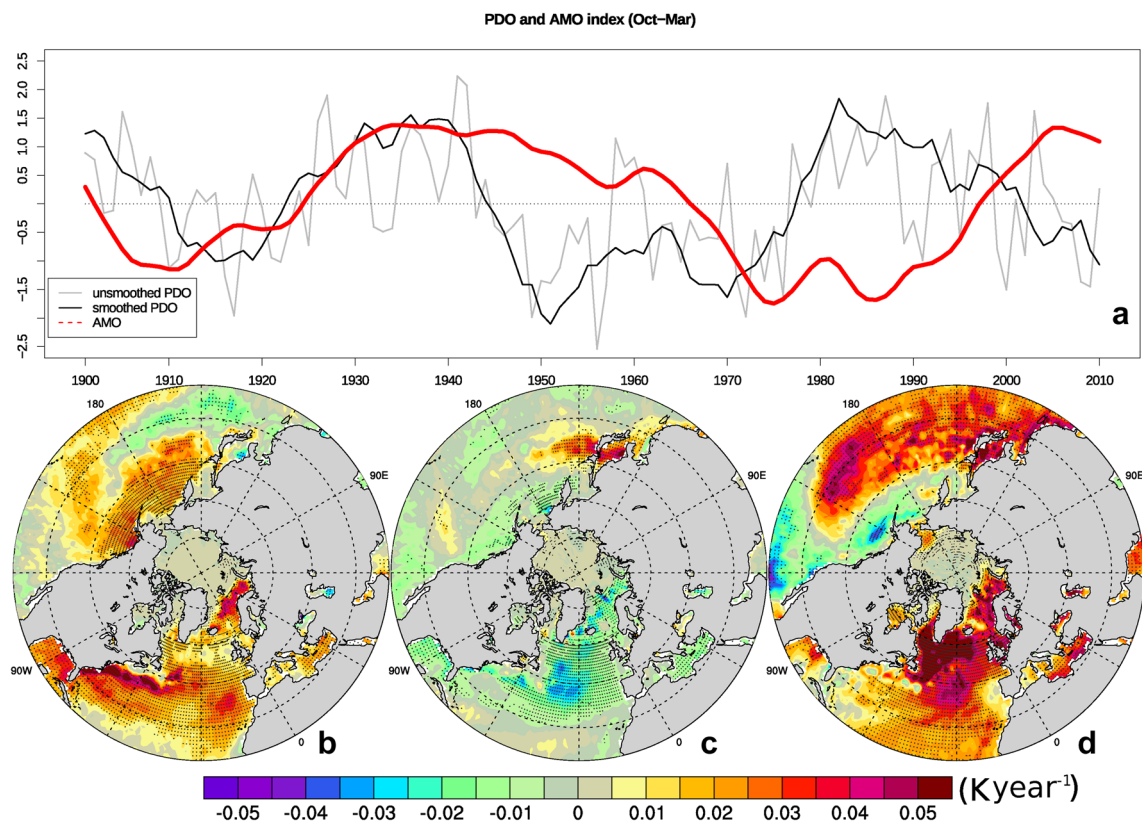
Fig. 10 **a** Twentieth century PDO/AMO indexes (continuous/dotted lines), spacial trends in SST for periods **b** I, **c** II and **d** III. Dotted grid points represent significant values with a minimum 95% confidence

AMO inversion from its extreme negative phase to a positive phase. Changes in the SST trend may have a dramatic impact on the storm-track since it can increase or reduce the low-level atmospheric temperature gradients and then the baroclinicity (Nakamura and Shimpo 2004).

During period I, the PDO index (black and grey line on Fig. 10a) has a minimum negative value in the mid 10s, and two maxima in early 1900 and in the mid 30s. Hence, there is no specific PDO trend during period I. Then, during period II, the PDO abruptly shifts from a strong positive phase in mid 30s to a strong negative phase in early 50s that lasts until the 70s and turns positive again until the late 80s. Hence, the SST trends of period II are well marked by the negative-minus-positive PDO anomalies (Fig. 10c). During period III, it decreases again from the peak in late 80s. Therefore, the two most important changing points of the PDO time series (1930 and 1980) go in agreement with the three periods defined for this article. But because period II is characterized by first an abrupt positive-to-negative PDO transition in the 40s and then an abrupt positive-to-negative AMO transition in the early 1970s, the period is split into two sub-periods: period IIa from 1935 until 1957 and period IIb from 1957 to 1980. Our hypothesis is that for period IIa, it is mainly the PAC region which drives storm-track

dynamics while for period IIb, it is mainly the ATL region. The next paragraphs aims at validating this hypothesis.

In the beginning of sub-period IIa, the PDO is positive and rapidly decreases. The cooler (warm) waters in central (north-east) PAC are then replaced by warm (cool) water. This is observed in SST trends shown in Fig. 11a and is more obvious than for the whole period II (Fig. 10c). At the very end of sub-period IIb, PDO changes again to positive phase and the SST pattern drives away from the previous pattern. In the ATL region, the transition from positive to negative AMO phase starts at the end of IIa and mainly occurs during IIb. The negative trends in SST are then more obvious in IIb, especially in a rather large area located south of Iceland near 60°N (Fig. 11b). There are also some positive trends in a narrower area along the east coast of the US in the Gulf Stream region.

Computation of the baroclinic conversion and baroclinicity for the two sub-periods confirms that PAC and ATL play a key role in storm-track dynamics for sub-periods IIa and IIb respectively (Fig. 11c–f). During IIa, when the PDO rapidly shifts toward its negative phase, the baroclinic conversion and baroclinicity increase north and decrease south of their peak amplitudes in PAC, consistent with SST gradient changes. Baroclinicity increase to the north covers a larger
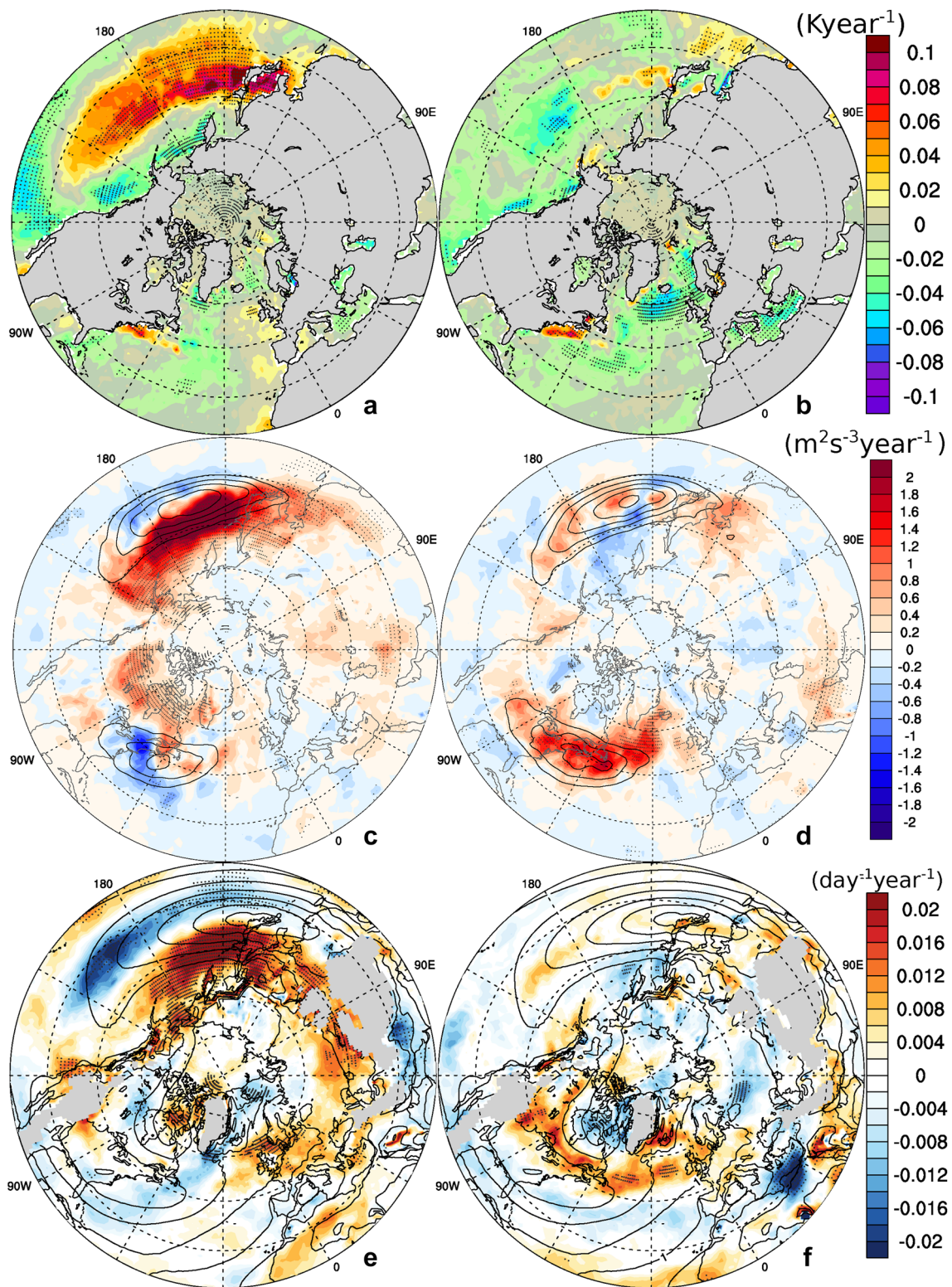
Fig. 11 **a**, **b** Sea surface temperature, **c**, **d** baroclinic conversion and **e**, **f** baroclinicity trends for (left column) period IIa and (right column) period IIb. Contours represent the mean field of the variable for each period in the same units as the trends (contour intervals of 25 m²s⁻³ and 0.5 day⁻¹ for baroclinic conversion and baroclinicity respectively). Dotted grid points represent significant values with a minimum 95% confidence
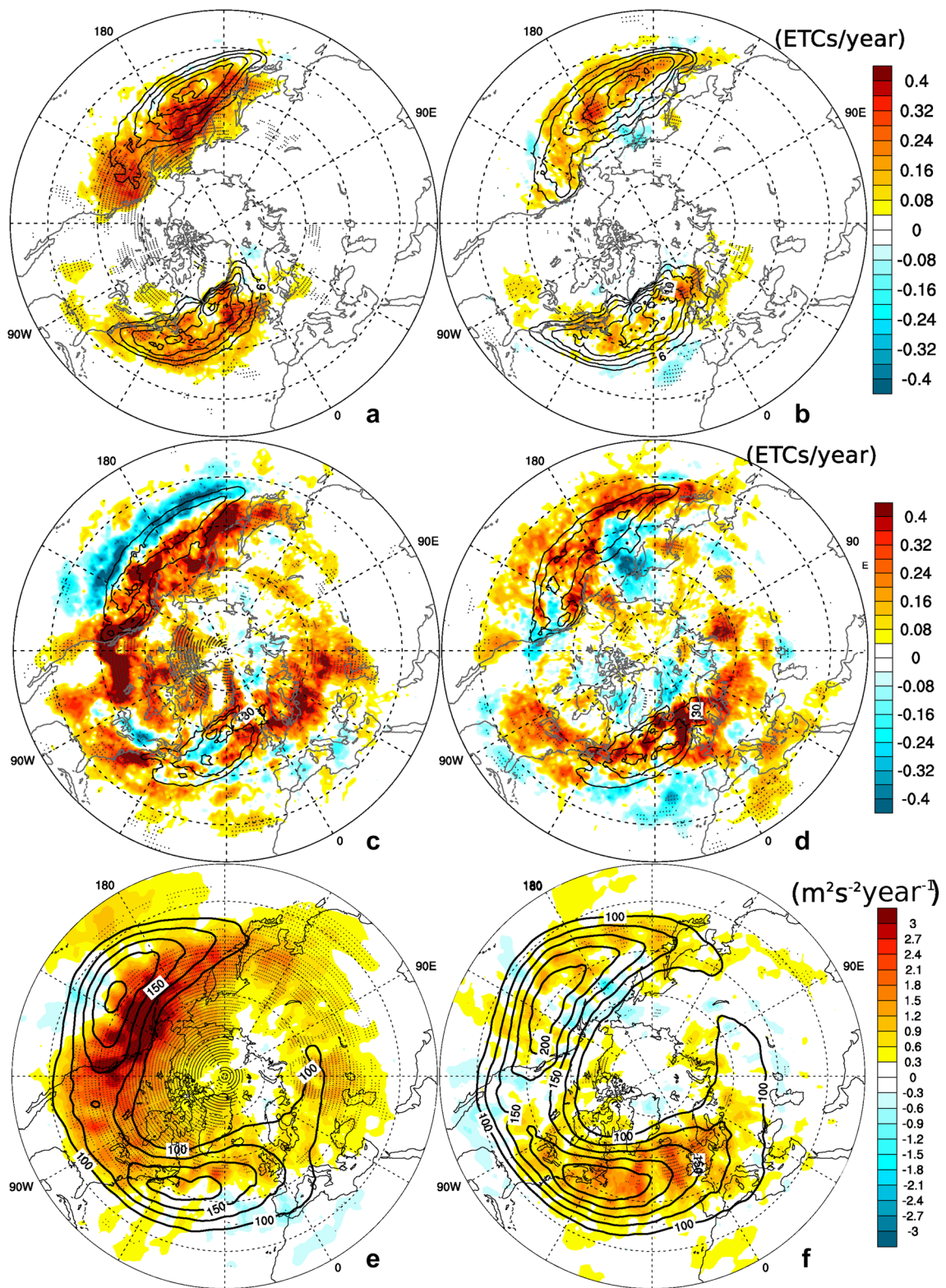
Fig. 12 Same as Fig. 10 but for **a**, **b** *Strong* ETCs **c**, **d** *All* ETCs and **e**, **f** 300 hPa EKE trends

area than the decrease to the south. Baroclinic conversion globally intensifies in PAC (Fig. 11c). This probably explains the strong increase in *Strong* ETC frequencies (Fig. 12a) and 300-hPa EKE (Fig. 12e) in PAC. Interestingly, the *All* ETC frequencies (Fig. 12c) exhibit a poleward-shifted storm-track while the *Strong* ETC frequencies (Fig. 12a) undergo an increase over all PAC regions showing that *Moderate* and *Strong* cyclones do not behave similarly. Generally speaking, these results go in agreement with studies that proved a good correlation between negative PDO and a northward-shifted and intensified PAC storm track (Lee et al. 2012; Sung et al. 2014; Gan and Wu 2013).

During IIa, in ATL, baroclinic conversion tendencies are positive over the Canada but there is no significant change in the baroclinic conversion intensity in the western Atlantic (Fig. 11c). Only some kind of poleward shift can be noticed. Trends in baroclinicity are non significant except over north-western Europe (Fig. 11e). However, all diagnoses quantifying the intensity of the storm-track eddy activity show a significant positive trend in ATL during IIa (Fig. 12a, c, e). Figure 12e gives us some insights: the upper-level high-frequency eddy kinetic energy shows a large positive trend over North America. Seeding of higher-amplitude upper-level disturbances fromed in the PAC and North American area could trigger more surface cyclones in the ATL sector and might explain the positive trend in ATL storm-track intensity. Another possibility would be that the increased cyclonic activity over the ATL ocean can be attributed to more seeding of surface cyclones having their incipient and main intensification stages over Northern America and the PAC area (Penny et al. 2013) as suggested by the important trend in *All* ETC frequencies (Fig. 12c) in that region. Note in particular that the strong increase in *All* ETC frequencies over North America comes from *Moderate* ETC frequencies as it is not present in *Strong* ETC frequencies (Fig. 12a) in that region but may then trigger *Strong* cyclones further downstream in the Atlantic sector where the mean baroclinicity is the strongest.

During IIb, the opposite is verified: the baroclinic conversion and baroclinicity trends are significantly positive at mid and high latitudes in ATL while no significant tendencies are observed in PAC (Fig. 11d, f). The baroclinicity increase along a band from Newfoundland to the British Isles is consistent with the increase in SST gradient in that sector due to the trend toward negative AMO. This explains the strong positive trend of the baroclinic conversion in the beginning of period IIa together with the global intensification and poleward-shifted of the Atlantic storm track, which is particularly obvious in *All* ETC frequencies (Fig. 12d), going in agreement with studies for the same period (Wang et al. 2006; Trigo 2006). Nevertheless, in the end of period II an increase in ATL baroclinicity is observed from 1970 up to the 1985 (see supplementary material), when the AMO

stops decreasing. A deeper analysis shows that there is still an increase in SST gradient in agreement with an increase in the low-level and vertically-averaged baroclinicity during that period (see supplementary material). Hence, there are SST anomalies that may have influenced the ATL storm-track that are not associated with a variation of the AMO index. In PAC, there is no important change in baroclinic conversion and baroclinicity compared to ATL (Fig. 11d, f). Some increase can be however noticed in eastern Asia or more downstream in mid-latitudes and may explain why the PAC storm-track is more intense in its core region. Some decrease in both the baroclinic conversion and baroclinicity appears more poleward, especially near the Kamchatka peninsula, which could explain the reduction in storm-track activity in that particular region as inferred from Fig. 12b, d, f.

6 On the potential impact of the non-homogeneous assimilated observations

Even though a good agreement is found between storm tracks, baroclinicity and large scale modes of variability, the impact of the increasing density of observations assimilated in the reanalysis on the trends observed in Fig. 1 must be assessed. In this perspective, we compare some diagnosis results between ERA20C and member 0 of ERA20CM (Hersbach et al. 2015), which is forced by the same SSTs and does not assimilate atmospheric observations. Figure 13a shows the number of all detected vorticity maxima without any threshold for ERA-20C and without considering the tracking algorithm. Such a number does not present any significant trend for any of the three periods. It therefore suggests there is no heterogeneity in the response to the increase in observation density in the reanalysis. In contrast, when only vorticity maxima greater than $2f_0$ are considered, a general increase is found in ERA-20C during period II as shown in Fig. 13b. This is consistent with the increased number of moderate-to-deep cyclone trajectories shown in Fig. 1a. Therefore, the detected trends for period II are only valid for cyclones having a significant amplitude. Another insight about the effect of assimilation is shown in Fig. 13c, which is the same diagnosis as Fig. 13b, but applied to ERA-20CM. The number of detected vorticity maxima is almost twice higher in ERA-20CM than in ERA-20C during the whole Century and even during period I when observations assimilated in ERA-20C are much fewer. Hence, during period I, the observations have already an important impact on the number of vorticity maxima but it is not clear if they constrain the atmospheric variables in the right way or not. To conclude, unlike the commonly accepted rationale, the addition of a great number of observations into the assimilation

Fig. 13 Time evolution of the pdfs of vorticity maxima in the Northern Hemisphere (20° N–90°N;180°W–180°E) for **a** all maxima in ERA-20C, **b** all maxima greater than $2f_0$ in ERA-20C, **c** same as **b** but in ERA-20CM (member 0). Black line: yearly-mean number of vorticity maxima detected in a radius of 225 km; colors rectangles: inter-quantile distribution of the number of vorticity maxima found every year using 3-hourly data
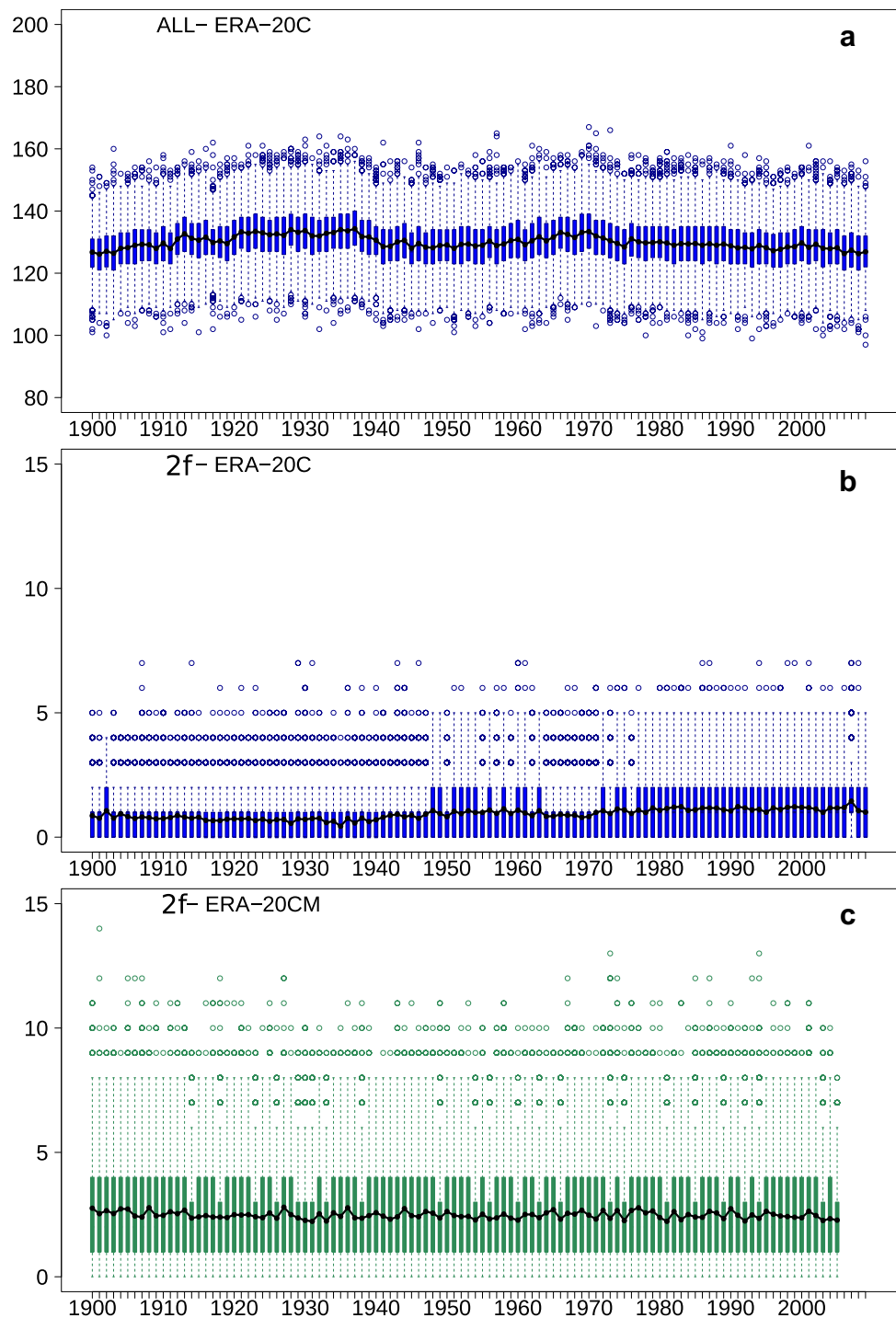
process does not lead to an increase in the number of vorticity maxima. Thus, the relationship between cyclonic activity and observation density is, for this reason, less trivial than expected.

When comparing ERA-20C with ERA-20CM, it is important to note that there is no trend in ERA-20CM which is not really surprising as the large-scale atmospheric variability significantly differs from ERA-20C (Poli et al. 2016, see

e.g., the NAO index in their Fig. 7c). It is not clear how this AMIP simulation accurately represents the response of the baroclinicity to SST AMO/PDO phase variations and further studies would be needed to investigate this particular aspect.

Further insights on the impact of the increased number of observations and the potential biases of ERA-20C can be gained when comparing to other reanalysis datasets during the second half of the 20th century (Wang et al. 2016; Chang

and Yau 2016). These studies emphasized that large inhomogeneities between the reanalysis datasets appear when the number of assimilated observations is small. One example is the Southern Hemisphere during the recent period when non satellite-derived observations were sparse. In this case, results of ERA-20C, (which does not include satellite-derived observations) are questioned. One may think that the NH Pacific in the early period can be thought of as being analogous to the Southern Hemisphere in the recent period in ERA-20C as it also has a limited number of observations. Moreover, the magnitude of the detected trend found in ERA-20C during the second period should be questioned as the previously two studies showed that ERA-20C presents stronger trends than in other reanalysis. It is almost twice higher for deep-cyclones when compared with 20CR in the entire century (Wang et al. 2016) and in general higher than other reanalysis as JRA55 for the period 1959–2010 (Chang and Yau 2016). The reader is referred to the previously cited papers for further information.

7 Conclusion

Mid-latitude wintertime cyclone variability during the Twentieth Century and over the Northern Hemisphere has been analysed by applying a cyclone tracking algorithm to ERA-20C reanalysis datasets. Three main periods have been distinguished and studied separately. We have observed that periods between 1900 and 1935 (period I) and between 1980 and 2010 (period III) were characterized by non-significant trends in ETCs in the NH whereas that between 1935 and 1980 (period II) was characterized by a significant positive trend.

Even though periods I and III are quite different, they bring some similarities: both were marked by an increase in polar temperatures and sea-ice loss, which was more pronounced and covering higher levels and lower latitudes in period III (Harvey et al. 2013; Woollings et al. 2014; Barnes and Polvani 2015; Polyakov and Johnson 2000; Yamanouchi 2011). It led to a reduction in the meridional gradients of temperature and consequently in the mid-latitude baroclinicity (Barnes and Polvani 2015) of the lower troposphere. In contrast, in the upper troposphere, the mid-latitude temperature gradients mainly increased during these two periods due to tropical warming (mainly for period III) and polar cooling near 200–300 hPa. These opposite tendencies of temperature gradients in the lower and upper troposphere are similar to those predicted by future climate scenarios. These tendencies exert opposite influences on storm-track and the net effect is quite uncertain (Butler et al. 2010; Rivière 2011; Shaw et al. 2016) as confirmed in the present study where no global trends were found during periods I and III.

However, more regional changes in the temperature gradients were found. For period I, there was a significant reduction in the North Pacific storm-track eddy activity and westerly jet intensity, especially on the southward flank of their climatological maximum values, which is a consequence of a strong decrease in baroclinicity further south. Over the ATL, no significant changes were noticed. For period III, the North Pacific storm-track shows a northeastward shift, a slight global increase in the various storm-track quantities, which can be attributed to a strong increase in the baroclinicity further north. The latter is probably due to a shift toward the negative phase of the PDO which increased the SST gradient on the northeastern side of the North Pacific basin. This is coherent with an increased intensity of the North Pacific jet stream at the same location (Barton and Ellis 2009). During period III, in the North Atlantic, the baroclinicity conversion significantly decreased in the core region and baroclinicity decreases on the northern flank of its climatological maximum value and increases on its southern flank. It led to an overall decrease in storm-track intensity at middle latitudes. This can be first attributed to the Arctic sea-ice reduction and Arctic warming, which decreases the temperature gradient at low levels. This result is consistent with the studies showing a negative NAO trend response to Arctic warming (Bader et al. 2011; Cohen et al. 2014; Nakamura et al. 2015; Oudar et al. 2016). This can be also attributed to a shift toward the positive phase of the AMO during that period which tends to shift the NAO toward its negative phase and decrease the storm-track intensity (Peings and Magnusdottir 2014; Peings et al. 2016).

Period II, between 1935 and 1980, was characterized by an increased intensity of both the North Pacific and North Atlantic storm tracks as measured by high-pass eddy kinetic energy and ETCs diagnostics. This positive trend can be explained by colder temperatures north of 50°N in connection with more ice cover (Box et al. 2009; Kinnard et al. 2008) that causes the meridional temperature gradient to homogeneously increase over the whole troposphere. Period II was marked by rapid shifts, first toward the negative phase of the PDO between 1935 and 1957 (period IIa), and then toward the negative phase of the AMO between 1957 and 1980 (period IIb). The shift toward the negative phase of the PDO in period IIa is responsible for the warming of the North Pacific ocean between 30°N and 45°N leading to strong increase in SST gradients and baroclinicity north of 45°N. In contrast, the decreased baroclinicity to the south of the Pacific warming is less important and extends over a smaller area. There is thus a poleward shift, together with an overall intensification, of the SST gradient, the baroclinicity and baroclinic conversion which explain the increased frequency of moderate-to-strong ETCs. The intensification of the North Pacific storm-track creates more upstream seeding of the North Atlantic storm-track. This may explain

why the ATL storm-track increases despite the fact that the baroclinicity and baroclinic conversion in the North Atlantic sector have no significant changes. During the second subperiod between 1957 and 1980, it is mainly the Atlantic sector which exhibits the strongest changes in SST gradient, baroclinicity and baroclinic conversion because of the shift toward the negative AMO phase. Similarly to the PDO structure, the transition toward the negative AMO phase creates an increase of all these quantities on the northern flank of their climatological maximum values and a decrease on the southern flank with the former increase being more intense than the latter decrease. For these reasons, the Atlantic storm-track therefore shifted poleward and mainly intensified between 1957 and 1980. Despite an overall intensification of the Pacific storm-track during the same subperiod, it cannot be attributed to well-marked changes of baroclinicity and baroclinic conversion in that region. One possibility is the stronger upstream seeding from the Atlantic storm-track but the signal does not seem to be very strong.

Some general conclusions about the impact of the AMO and PDO on storm-track dynamics can be deduced from the present study. The negative (positive) phases of the AMO and PDO tends to intensify (decrease) and shift poleward (equatorward) the baroclinicity, baroclinic conversion and storm-track quantities of the North Atlantic and North Pacific sectors respectively. This confirms other studies on the topic (Peings and Magnusdottir 2014; Peings et al. 2016; Gan and Wu 2013). This may explain why period III which is marked by a negative PDO trend and a positive AMO trend show opposite tendencies in the Pacific and Atlantic sectors and there is no net change in storm-track dynamics over the whole hemisphere. In contrast, period II is well marked by negative trends in both PDO and AMO indexes that create a net intensification of the Northern Hemisphere storm tracks. To conclude, multi-decadal variabilities during the 20th century of the storm-track and baroclinicity are closely connected and largely depends on decadal oceanic variability patterns as the AMO and PDO. For some periods as periods I and III, the Pacific and Atlantic response is not the same and even tend to oppose to each other which means that hemispheric analysis may not be enough to take general conclusions about the storm-tracks. In contrast, for period II, the tendencies of the two regions tend to add to each other. Of course, this is a quite general picture and the basic knowledge of the PDO and AMO indexes is not enough to understand the structure of the SST anomalies and their impact on the atmosphere as seen for instance in the North Atlantic case at the end of period IIb (supplementary material).

Other general statements can be made about the impact of global warming on storm-track dynamics. First, we found an overall reduction in the Atlantic storm-track activity and a poleward-shift and intensification of the Pacific storm track during period III, consistent with Wang et al. (2017). Our interpretation is mainly based on the transitions toward negative PDO and positive AMO, but the role of these multidecadal modes of ocean variability should be separated from that of the Arctic amplification to quantitatively assess their impacts in future studies. Another statement can be made about the vertical structure of the trends under global warming. Despite a rapid warming of the polar regions in period III after the 1980s, the decrease in the horizontal temperature gradients and the baroclinicity is rather confined to the lower troposphere and its effect seems to be partly compensated by that of the increased upper-tropospheric temperature gradients. This is to be contrasted with period II between 1935 and 1980 where the moderate cooling in polar regions extends from the surface to the upper troposphere and more homogeneously increases the horizontal temperature gradients in mid-latitudes. As such, the effect of this moderate polar cooling on storm-track appears to be more important. Hence, the effect of polar temperature anomalies on storm-track strongly depends on their spatial patterns and how they extend over the whole troposphere. This should be kept in mind when considering the storm-track response to global warming.

Finally, we have discussed the time inhomogeneity on the amount of observations in ERA-20C. An observation-related trend potentially exists in long-term reanalysis datasets as mentioned by some authors and an overestimation of the period II ETC's positive trends could be a consequence. A comparison between ERA-20C and ERA-20CM was made in order to compare the corresponding trends. Despite to what could be expected from an increased number of assimilated observations, the total number of vorticity maxima detected in ERA-20C does not increase with time. Furthermore, the number of vorticity maxima is in general higher in ERA-20CM than in ERA-20C. The data assimilation system in the presence of dense observations networks can reduce the synoptic activity when the free model does produce too much spurious cyclones. Its real effect is less trivial then expected and could not be fully addressed without further studies. Finally, even though the use of long-term reanalysis must be done with caution, we have shown that conclusive and coherent results can be extracted from this data, regardless the time inhomogeneity of the observations. First, some of these trends are consistent with those found in recent studies: the increase in cyclone counts from ERA-20C reanalyses (Chang and Yau 2016), the generalised cold tropospheric and SST temperatures (Box et al. 2009; Kinnard et al. 2008) and the increased jet strength (Woollings et al. 2014; Barton and Ellis 2009) during period II. Second, we have shown that the ETC trends are consistent with trends in other storm-track diagnostics and, more importantly, can be explained by variations in baroclinicity and large-scale modes of climate variability. The link found between the

synoptic eddy variability and the large-scale baroclinicity is not fully conclusive in itself as both fields might have biases/errors that go together. However, the fact that we also found a link with the rather well-documented 20th century multi-decadal ocean variations gives us more reliability on the sign of the detected trends despite the inhomogeneity of the assimilated observations. Still, one should keep in mind that only a qualitative analysis is made in this study. Even though the positive trend in the middle century is in agreement with several large-scale modes of climate variability, ERA-20C presents trends that are higher than other reanalysis (Chang and Yau 2016), that were not quantitatively explained here. For this reason we cannot exclude a possible overestimation of the trends due inhomogeneity of the assimilated observations, particularly in the middle century.

References

Ayrault F (1998) Environnment, structure et évolution des dépressions météorologiques: réalité climatologique et modèles types. Doctoral Dissertation. Universite Paul Sabatier, Meteo-France, Centre National de Recherches Météorologiques

Ayrault F, Joly A (2000) The genesis of mid-latitude cyclones over the Atlantic Ocean: a new climatological perspective. C R Acad Sci Paris Earth Planet Sci 330:173–178

Bader J, Mesquita MD, Hodges KI, Keenlyside N, Sterhus S, Miles M (2011) A review on Northern Hemisphere sea-ice, storminess and the North Atlantic oscillation: observations and projected changes. Atmos Res 101(4):809–834. https://doi.org/10.1016/j.atmosres.2011.04.007

Barnes EA, Polvani LM (2015) CMIP5 projections of Arctic amplification, of the North American/North Atlantic circulation, and of their relationship. J Clim 28(13):5254–5271. https://doi.org/10.1175/JCLI-D-14-00589.1

Barnes EA, Screen JA (2015) The impact of Arctic warming on the midlatitude jet-stream: can it? Has it? Will it?: impact of Arctic warming on the midlatitude jet-stream. Wiley Interdiscip Rev Clim Change 6(3):277–286. https://doi.org/10.1002/wcc.337

Barton NP, Ellis AW (2009) Variability in wintertime position and strength of the North Pacific jet stream as represented by re-analysis data. Int J Climatol 29:851–862. https://doi.org/10.1002/joc.1750

Bengtsson L (2004) Can climate trends be calculated from reanalysis data? J Geophys Res. https://doi.org/10.1029/2004JD004536

Bengtsson L, Hodges KI, Roeckner E (2006) Storm tracks and climate change. J Clim 19(15):3518–3543. https://doi.org/10.1175/JCLI3815.1

Blackmon ML, Wallace JM, Lau NC, Mullen SL (1977) An observational study of the Northern Hemisphere wintertime circulation. J Atmos Sci 34(7):1040–1053. https://doi.org/10.1175/1520-0469(1977)034<1040:AOSOTN>2.0.CO;2

Box JE, Yang L, Bromwich DH, Bai LS (2009) Greenland ice sheet surface air temperature variability: 1840–2007. J Clim 22(14):4029–4049. https://doi.org/10.1175/2009JCLI2816.1

Bromwich DH, Fogt RL, Hodges KI, Walsh JE (2007) A tropospheric assessment of the ERA-40, NCEP, and JRA-25 global reanalyses in the polar regions. J Geophys Res. https://doi.org/10.1029/2006JD007859

Butler A, Thompson D, Heikes R (2010) The steady-state atmospheric circulation response to climate change-like thermal forcings in a simple general circulation model. J Clim 23:3474–3496. https://doi.org/10.1175/2010JCLI3228.1

Cattiaux J, Cassou C (2013) Opposite CMIP3/CMIP5 trends in the wintertime northern annular mode explained by combined local sea ice and remote tropical influences. Geophys Res Lett 40:3682–3687. https://doi.org/10.1002/grl.50643

Cattiaux J, Vautard R, Cassou C, Yiou P, Masson-Delmotte V, Codron F (2010) Winter 2010 in Europe: a cold extreme in a warming climate. Geophys Res Lett 37:L20704. https://doi.org/10.1029/2010GL044613

Chang EKM (2007) Assessing the increasing trend in Northern Hemisphere winter storm track activity using surface ship observations and a statistical storm track model. J Clim 20(22):5607–5628. https://doi.org/10.1175/2007JCLI1596.1

Chang EKM, Fu Y (2002) Interdecadal variations in Northern Hemisphere winter storm track intensity. J Clim 15(6):642–658. https://doi.org/10.1175/1520-0442(2002)015<0642:IVINHW>2.0.CO;2

Chang EKM, Fu Y (2003) Using mean flow change as a proxy to infer interdecadal storm track variability. J Clim 16:2178–2196

Chang EKM, Yau AMW (2015) Northern Hemisphere winter storm track trends since 1959 derived from multiple reanalysis datasets. Clim Dyn 47(5–6):1435–1454. https://doi.org/10.1007/s00382-015-2911-8

Chang EKM, Yau AMW (2016) Northern Hemisphere winter storm track trends since 1959 derived from multiple reanalysis datasets. Clim Dyn 47(5):1435–1454. https://doi.org/10.1007/s00382-015-2911-8

Chang EKM, Lee S, Swanson KL (2002) Storm track dynamics. J Clim 15(16):2163–2183. https://doi.org/10.1175/1520-0442(2002)015<02163:STD>2.0.CO;2

Chang EKM, Guo Y, Xia X (2012) CMIP5 multimodel ensemble projection of storm track change under global warming. J Geophys Res Atmos 117(D23):D23,118. https://doi.org/10.1029/2012JD018578

Cohen J, Screen JA, Furtado JC, Barlow M, Whittleston D, Coumou D, Francis J, Dethloff K, Entekhabi D, Overland J, Jones J (2014) Recent arctic amplification and extreme mid-latitude weather. Nat Geosci 7:627–637. https://doi.org/10.1038/ngeo2234

Compo GP, Whitaker JS, Sardeshmukh PD, Matsui N, Allan RJ, Yin X, Gleason BE, Vose RS, Rutledge G, Bessemoulin P, Brnnimann S, Brunet M, Crouthamel RI, Grant AN, Groisman PY, Jones PD, Kruk MC, Kruger AC, Marshall GJ, Maugeri M, Mok HY, Nordli Ross TF, Trigo RM, Wang XL, Woodruff SD, Worley SJ (2011) The twentieth century reanalysis project. Q J R Meteorol Soc 137(654):1–28. https://doi.org/10.1002/qj.776

Corti S, Molteni F, Palmer T (1999) Signature of recent climate change in frequencies of natural atmospheric circulation regimes. Nature 398:799–802. https://doi.org/10.1038/19745

Dell'Aquila A, Corti S, Weisheimer A, Hersbach H, Peubey C, Poli P, Berrisford P, Dee D, Simmons A (2016) Benchmarking Northern Hemisphere midlatitude atmospheric synoptic variability in centennial reanalysis and numerical simulations. Geophys Res Lett 43(10):5442–5449. https://doi.org/10.1002/2016GL068829

Enfield DB, Mestas-Nuez AM, Trimble PJ (2001) The Atlantic multi-decadal oscillation and its relation to rainfall and river flows in the continental US. Geophys Res Lett 28(10):2077–2080. https://doi.org/10.1029/2000GL012745

Gan B, Wu L (2013) Seasonal and long-term coupling between wintertime storm tracks and sea surface temperature in the North Pacific. J Climate 26(16):6123–6136. https://doi.org/10.1175/JCLI-D-12-00724.1

Gastineau G, Frankignoul C (2015) Influence of the North Atlantic SST variability on the atmospheric circulation during the twentieth century. J Clim 28:1396–1416. https://doi.org/10.1175/JCLI-D-14-00424.1

Geng Q, Sugi M (2003) Possible change of extratropical cyclone activity due to enhanced greenhouse gases and sulfate aerosols—study with a high-resolution AGCM. J Clim 16(13):2262–2274. https://doi.org/10.1175/1520-0442(2003)16<2262:PCOECA>2.0.CO;2

Gomara I, Rodriguez-Fonseca B, Zurita-Gotor P, Ulbrich S, Pinto JG (2016) Abrupt transitions in the NAO control of explosive North Atlantic cyclone development. Clim Dyn 47:3091–3111. https://doi.org/10.1007/s00382-016-3015-9

Graham NE, Diaz HF (2001) Evidence for intensification of North Pacific winter cyclones since 1948. Bull Am Meteorol Soc 82(9):1869–1893. https://doi.org/10.1175/1520-0477(2001)082<1869:EFIONP>2.3.CO;2

Gulev SK, Zolina O, Grigoriev S (2001) Extratropical cyclone variability in the Northern Hemisphere winter from the NCEP/NCAR reanalysis data. Clim Dyn 17(10):795–809. https://doi.org/10.1007/s003820000145

Harvey BJ, Shaffrey LC, Woollings TJ (2013) Equator-to-pole temperature differences and the extra-tropical storm track responses of the CMIP5 climate models. Clim Dyn 43(5–6):1171–1182. https://doi.org/10.1007/s00382-013-1883-9

Hersbach H, Peubey C, Simmons A, Berrisford P, Poli P, Dee D (2015) ERA-20cm: a twentieth-century atmospheric model ensemble: the ERA-20cm ensemble. Quart J R Meteorol Soc 141(691):2350–2375. https://doi.org/10.1002/qj.2528

Hoskins BJ, Hodges KI (2002) New perspectives on the Northern Hemisphere winter storm tracks. J Atmos Sci 59(6):1041–1061. https://doi.org/10.1175/1520-0469(2002)059<1041:NPOTNH>2.0.CO;2

Hoskins BJ, Valdes PJ (1990) On the existence of storm-tracks. J Atmos Sci 47(15):1854–1864. https://doi.org/10.1175/1520-0469(1990)047<1854:OTEOST>2.0.CO;2

Kinnard C, Zdanowicz CM, Koerner RM, Fisher DA (2008) A changing Arctic seasonal ice zone: observations from 1870–2003 and possible oceanographic consequences. Geophys Res Lett. https://doi.org/10.1029/2007GL032507

Krueger O, Schenk F, Feser F, Weisse R (2013) Inconsistencies between long-term trends in storminess derived from the 20cr reanalysis and observations. J Clim 26(3):868–874. https://doi.org/10.1175/JCLI-D-12-00309.1

Lee SS, Lee JY, Wang B, Ha KJ, Heo KY, Jin FF, Straus DM, Shukla J (2012) Interdecadal changes in the storm track activity over the North Pacific and North Atlantic. Clim Dyn 39(1–2):313–327. https://doi.org/10.1007/s00382-011-1188-9

L'Heureux M, Butler A, Jha B, Kumer A, Wang W (2010) Unusual extremes in the negative phase of the Arctic Oscillation during 2009. Geophys Res Lett 37:L10,704. https://doi.org/10.1029/2010GL043338

Mantua NJ, Hare SR, Zhang Y, Wallace JM, Francis RC (1997) A Pacific interdecadal climate oscillation with impacts on salmon production. Bull Am Meteorol Soc 78(6):1069–1079. https://doi.org/10.1175/1520-0477(1997)078<1069:APICOW>2.0.CO;2

McCabe GJ, Clark MP, Serreze MC (2001) Trends in Northern Hemisphere surface cyclone frequency and intensity. J Clim 14(12):2763–2768. https://doi.org/10.1175/1520-0442(2001)014<2763:TINHSC>2.0.CO;2

McDonald RE (2010) Understanding the impact of climate change on Northern Hemisphere extra-tropical cyclones. Clim Dyn 37(7–8):1399–1425. https://doi.org/10.1007/s00382-010-0916-x

Michel C, Rivière G, Terray L, Joly B (2012) The dynamical link between surface cyclones, upper-tropospheric Rossby wave breaking and the life cycle of the Scandinavian blocking. Geophys Res Lett 39(10):10806. https://doi.org/10.1029/2012GL051682

Nakamura T, Yamazaki K, Iwamoto K, Honda M, Miyoshi Y, Ogawa Y, Ukita J (2015) A negative phase shift of the winter AO/NAO due to the recent Arctic sea-ice reduction in late autumn: negative shift of AO by ARCTIC ice loss. J Geophys Res Atmos 120(8):3209–3227. https://doi.org/10.1002/2014JD022848

Nakamura TSYT H, Shimpo A (2004) Observed associations among storm tracks, jet streams and midlatitude oceanic fronts. vol Earth's climate: the ocean-atmosphere interaction. In: Wang C, Xie SP, Carton JA (eds) Geophys Monogr Ser, pp 329–345. https://doi.org/10.1029/147GM18

Neu U, Akperov MG, Bellenbaum N, Benestad R, Blender R, Caballero R, Cocozza A, Dacre HF, Feng Y, Fraedrich K, Grieger J, Gulev S, Hanley J, Hewson T, Inatsu M, Keay K, Kew SF, Kindem I, Leckebusch GC, Liberato MLR, Lionello P, Mokhov II, Pinto JG, Raible CC, Reale M, Rudeva I, Schuster M, Simmonds I, Sinclair M, Sprenger M, Tilinina ND, Trigo IF, Ulbrich S, Ulbrich U, Wang XL, Wernli H (2013) IMILAST: a community effort to intercompare extratropical cyclone detection and tracking algorithms. Bull Am Meteorol Soc 94(4):529–547. https://doi.org/10.1175/BAMS-D-11-00154.1

Oudar T, Sanhez-Gomez E, Chauvin F, Cattiaux J, Cassou C, Terray L (2016) Respective roles of direct radiative forcing and induced Arctic sea ice loss on the Northern Hemisphere atmospheric circulation. Clim Dyn. https://doi.org/10.1007/s00382-017-3541-0 (in revision)

Paciorek CJ, Risbey JS, Ventura V, Rosen RD (2002) Multiple indices of Northern Hemisphere cyclone activity, winters 194999. J Clim 15(13):1573–1590. https://doi.org/10.1175/1520-0442(2002)015<1573:MIONHC>2.0.CO;2

Peings Y, Magnusdottir G (2014) Forcing of the wintertime atmospheric circulation by the multidecadal fluctuations of the North Atlantic ocean. Environ Res Lett 9:034018. https://doi.org/10.1088/1748-9326/9/3/034018

Peings Y, Simpkins G, Magnusdottir G (2016) Multidecadal fluctuations of the North Atlantic ocean and feedback on the winter climate in CMIP5 control simulations. J Geophys Res Atmos 121:2571–2592. https://doi.org/10.1002/2015JD024107

Penny SM, Battisti DS, Roe GH (2013) Examining mechanisms of variability within the Pacific storm track: upstream seeding and jet-core strength. J Clim 26(14):5242–5259. https://doi.org/10.1175/JCLI-D-12-00017.1

Pinto J, Ulbrich U, Leckebush GC, Spangehl T, Reyers M, Zacharias S (2007) Changes in storm track and cyclone activity in three SRES ensemble experiments with the ECHAM5/MPI-OM1 GCM. Clim Dyn 29:195–210. https://doi.org/10.1007/s00382-007-0230-4

Poli P, Hersbach H, Dee DP, Berrisford P, Simmons AJ, Vitart F, Laloyaux P, Tan DGH, Peubey C, Thpaut JN, Trmolet Y, Hlm EV, Bonavita M, Isaksen L, Fisher M (2016) ERA-20c: an atmospheric reanalysis of the twentieth century. J Clim 29(11):4083–4097. https://doi.org/10.1175/JCLI-D-15-0556.1

Polyakov IV, Johnson MA (2000) Arctic decadal and interdecadal variability. Geophys Res Lett 27(24):4097–4100. https://doi.org/10.1029/2000GL011909

Rahmstorf S, Box JE, Feulner G, Mann ME, Robinson A, Rutherford S, Schaffernicht EJ (2015) Exceptional twentieth-century slowdown in Atlantic Ocean overturning circulation. Nat Clim Chang 5(5):475–480. https://doi.org/10.1038/nclimate2554

Raible CC, Della-Marta PM, Schwierz C, Wernli H, Blender R (2008) Northern Hemisphere extratropical cyclones: a comparison of detection and tracking methods and different reanalyses. Mon Weather Rev 136(3):880–897. https://doi.org/10.1175/2007MWR2143.1

Rivière G (2011) A dynamical interpretation of the poleward shift of the jet streams in global warming scenarios. J Atmos Sci 68(6):1253–1272. https://doi.org/10.1175/2011JAS3641.1

Rivière G, Drouard M (2015) Dynamics of the northern annular mode at weekly time scales. J Atmos Sci 72:4569–4590. https://doi.org/10.1175/JAS-D-15-0069.1

Rivière G, Joly A (2006) Role of the low-frequency deformation field on the explosive growth of extratropical cyclones at the jet exit.

Part I: barotropic critical region. J Atmos Sci 63(8):1965–1981. https://doi.org/10.1175/JAS3728.1

Rivière G, Hua BL, Klein P (2004) Perturbation growth in terms of baroclinic alignment properties. Q J R Meteorol Soc 130(600):1655–1673. https://doi.org/10.1256/qj.02.223

Shaffrey L, Sutton R (2006) Bjerknes compensation and the decadal variability of the energy transports in a coupled climate model. J Clim 19(7):1167–1181. https://doi.org/10.1175/JCLI3652.1

Shaw T, Baldwin M, Barnes E, Caballero R, Garfinkel C, Hwang YT, Li C, O'Gorman P, Rivière G, Simpson I, Voigt A (2016) Storm track processes and the opposing influences of climate change. Nat Geosci 9:656–664. https://doi.org/10.1038/ngeo2783

Sinclair MR (1997) Objective identification of cyclones and their circulation intensity, and climatology. Weather Forecast 12(3):595–612. https://doi.org/10.1175/1520-0434(1997)012<0595:OIOCAT>2.0.CO;2

Sung MK, An SI, Kim BM, Woo SH (2014) A physical mechanism of the precipitation dipole in the western United States based on PDO-storm track relationship: precipitation dipole in the western US. Geophys Res Lett. https://doi.org/10.1002/2014GL060711

Theil H (1950) A rank-invariant method of linear and polynomial regression analysis. i, ii, iii. Nederl Akad Wetensch. Proc 53 130:386392

Thompson DWJ, Wallace JM (1998) The Arctic Oscillation signature in the wintertime geopotential height and temperature fields. Geophys Res Lett 25:1297–1300. https://doi.org/10.1029/98GL00950

Tilinina N, Gulev SK, Rudeva I, Koltermann P (2013) Comparing cyclone life cycle characteristics and their interannual variability in different reanalyses. J Clim 26(17):6419–6438. https://doi.org/10.1175/JCLI-D-12-00777.1

Trigo IF (2006) Climatology and interannual variability of storm-tracks in the Euro-Atlantic sector: a comparison between ERA-40 and NCEP/NCAR reanalyses. Clim Dyn 26(2–3):127–143. https://doi.org/10.1007/s00382-005-0065-9

Ulbrich U, Leckebusch GC, Pinto JG (2009) Extra-tropical cyclones in the present and future climate: a review. Theor Appl Climatol 96(1–2):117–131. https://doi.org/10.1007/s00704-008-0083-8

Wang J, Kim HM, Chang EKM (2017) Changes in Northern Hemisphere winter storm tracks under the background of Arctic amplification. J Clim 30(10):3705–3724. https://doi.org/10.1175/JCLI-D-16-0650.1

Wang XL, Swail VR, Zwiers FW (2006) Climatology and changes of extratropical cyclone activity: comparison of ERA-40 with NCEP-NCAR reanalysis for 19582001. J Clim 19(13):3145–3166. https://doi.org/10.1175/JCLI3781.1

Wang XL, Feng Y, Compo GP, Swail VR, Zwiers FW, Allan RJ, Sardeshmukh PD (2013) Trends and low frequency variability of extra-tropical cyclone activity in the ensemble of twentieth century reanalysis. Clim Dyn 40(11–12):2775–2800. https://doi.org/10.1007/s00382-012-1450-9

Wang XL, Feng Y, Chan R, Isaac V (2016) Inter-comparison of extra-tropical cyclone activity in nine reanalysis datasets. Atmos Res 181:133–153. https://doi.org/10.1016/j.atmosres.2016.06.010

Woollings T, Gregory JM, Pinto JG, Reyers M, Brayshaw DJ (2012) Response of the North Atlantic storm track to climate change shaped by ocean–atmosphere coupling. Nat Geosci 5(5):313–317. https://doi.org/10.1038/ngeo1438

Woollings T, Czuchnicki C, Franzke C (2014) Twentieth century North Atlantic jet variability. Q J R Meteorol Soc 140(680):783–791. https://doi.org/10.1002/qj.2197

Yamamoto A, Palter JB (2016) The absence of an Atlantic imprint on the multidecadal variability of wintertime European temperature. Nat Commun 7(10):930. https://doi.org/10.1038/ncomms10930

Yamanouchi T (2011) Early 20th century warming in the Arctic: a review. Polar Sci 5(1):53–71. https://doi.org/10.1016/j.polar.2010.002

Zappa G, Shaffrey LC, Hodges KI, Sansom PG, Stephenson DB (2013) A multimodel assessment of future projections of North Atlantic and European extratropical cyclones in the CMIP5 climate models. J Clim 26(16):5846–5862. https://doi.org/10.1175/JCLI-D-12-00573.1